**TCR meta-clonotypes for biomarker discovery with tcrdist3: identification of public, HLA-restricted SARS-CoV-2 associated TCR features**

Koshlan Mayer-Blackwell[1], Stefan Schattgen[2], Liel Cohen-Lavi[3,4], Jeremy Chase Crawford[2], Aisha Souquette[2], Jessica A. Gaevert[2,5], Tomer Hertz[6], Paul G. Thomas[2], Philip Bradley[7], Andrew Fiore-Gartland[1]

[1] Vaccine and Infectious Disease Division, Fred Hutchinson Cancer Research Center, Seattle, USA

[2] Immunology Department, St. Jude Children's Research Hospital, Memphis, USA

[3] Department of Industrial Engineering and Management, Ben-Gurion University of the Negev, Be'er-Sheva, Israel

[4] National Institute for Biotechnology in the Negev, Ben-Gurion University of the Negev, Be'er-Sheva, Israel

[5] St. Jude Graduate School of Biomedical Sciences, St. Jude Children's Research Hospital, Memphis, USA

[6] Shraga Segal Department of Microbiology and Immunology, Ben-Gurion University of the Negev, Be'er Sheva, Israel

[7] Public Health Science Division, Fred Hutchinson Cancer Research Center, Seattle, USA

**ABSTRACT**

As the mechanistic basis of adaptive cellular antigen recognition, T cell receptors (TCRs) encode clinically valuable information that reflects prior antigen exposure and potential future response. However, despite advances in deep repertoire sequencing, enormous TCR diversity complicates the use of TCR clonotypes as clinical biomarkers. We propose a new framework that leverages antigen-enriched repertoires to form meta-clonotypes – groups of biochemically similar TCRs – that can be used to robustly identify and quantify functionally similar TCRs in bulk repertoires. We apply the framework to TCR data from COVID-19 patients, generating 1831 public TCR meta-clonotypes from the 17 SARS-CoV-2 antigen-enriched repertoires with the strongest evidence of HLA-restriction. Applied to independent cohorts, meta-clonotypes targeting these specific epitopes were more frequently detected in bulk repertoires compared to exact amino acid matches, and 59.7% (1093/1831) were more abundant among COVID-19 patients that expressed the putative restricting HLA allele (FDR < 0.01), demonstrating the potential utility of meta-clonotypes as antigen-specific features for biomarker development. To enable further applications, we developed an open-source software package, *tcrdist3,* that implements this framework and facilitates flexible workflows for distance-based TCR repertoire analysis.

**INTRODUCTION**

An individual's unique repertoire of T cell receptors (TCRs) is shaped by antigen exposure and is a critical component of immunological memory, contributing to recall responses against future infectious challenges (Emerson et al., 2017; Welsh and Selin, 2002). With the advancement of immune repertoire profiling, TCR repertoires are a largely untapped source of biomarkers that could potentially be used to predict immune responses to a wide range of exposures including viral infections (Wolf et al., 2018), tumor neoantigens (Ahmadzadeh et al., 2019; Chiou et al., 2021; Kato et al., 2018), or environmental allergens (Cao et al., 2020). The TCR repertoire is characterized by its extreme diversity, originating from the genomic V(D)J gene recombination of receptors in development. Between $10^9$-$10^{10}$ unique clonotypes - T cells with distinct nucleotide-encoded receptors - are maintained in an adult human TCR repertoire (Lythe et al., 2016). The diversity, both within and between individuals, presents major hurdles to biomarker development. Researchers have used antigen-enrichment of T cell repertoires (e.g. peptide-major histocompatibility complex (MHC) tetramer sorting) to focus on TCR diversity of relevant targets, however this experimental strategy, which depends on knowing the peptide antigen and it's MHC restriction reveals the breadth of potential TCRs able to recognize even a single antigen (Coles et al., 2020; Meysman et al., 2019), which complicates detection of population-wide signatures of antigen exposure. Indeed, mathematical modeling suggests that only 10-15% of single chain TCRs are public or shared frequently by multiple individuals (Elhanati et al., 2018), which is consistent with observations from extremely deeply sequenced human repertoires (Soto et al., 2019). Despite advances in high-throughput next-generation TCR amplicon sequencing, only a fraction of the repertoire can be assayed, making it difficult to reproducibly sample many relevant TCR clonotypes from an individual, let alone reliably detect public clonotypes in a population. In practice, the problem is exacerbated by unequal sampling depth. Thus, individual T cell clonotypes are currently sub-optimal and under-powered for population-level investigations of TCR specificity, which limits their application in the development of TCR-based clinical biomarkers**.**

In this study we used antigen enriched TCR repertoires to form "meta-clonotypes": groups of TCRs with biochemically similar complementarity determining regions (CDRs) that likely share antigen recognition. Meta-clonotypes were implemented using a centroid TCR sequence and a biochemical radius that determines whether other TCRs are sufficiently similar to be grouped together; the appropriate radius was determined by comparing the proportion of similar TCRs in antigen-enriched and unenriched data. A CDR3 "motif" is also constructed from the TCRs within the radius, which further refines the specificity of meta-clonotype definition. Together the radius and the motif can be used to search for conformant TCRs in large bulk-sequenced repertoires and quantify their abundance (Figure 1). We find that TCR centroids, which are often private, gain publicity as meta-clonotypes.

The expanded publicity of meta-clonotypes provides an opportunity to develop population-level biomarkers of clinical outcomes that depend on antigen-specific features of the TCR repertoire, such as disease severity in natural infection or the level of vaccine-induced protection. Shifting the focus of repertoire analysis from clonotypes to meta-clonotypes increases statistical power by reducing the inherent sparsity of finite repertoire samples and increasing the precision with which antigen-specific cell abundance can be estimated. A number of existing tools enable grouping of TCRs by sequence similarity (Table S1); for example, VDJtools (TCRNET) and ALICE evaluate networks of similar TCR β- or TCR α-chain CDR3s based on a maximum edit-distance of one amino acid substitution, insertion or deletion,

74    while GLIPH2 groups similar TCRs based on shared amino acid k-mers in identical length CDR3s
75    (Glanville et al., 2017; Huang et al., 2020; Pogorelyy et al., 2019; Pogorelyy and Shugay, 2019; Ritvo et
76    al., 2018; Shugay et al., 2015). Previously, we introduced TCRdist, a weighted multi-CDR, biochemically
77    informed distance metric that enabled grouping of paired αβ TCRs by antigen specificity, based on their
78    sequence similarity (Dash et al., 2017). Here, we describe a new application of TCRdist that guides
79    formation of meta-clonotypes optimized for biomarker development. This application is made possible by
80    a new open-source Python3 software package *tcrdist3* that brings new flexibility to distance-based
81    repertoire analysis, allowing customization of the distance metric, analysis of γδ TCRs, and at-scale
82    computation with sparse data representations and parallelized, byte-compiled code.

83        Here we first describe a novel analytical framework for identifying meta-clonotypes in antigen-
84    enriched repertoires. The framework is then applied to a large publicly available dataset of putative
85    SARS-CoV-2 antigen-associated TCRs with the objective of identifying meta-clonotypes that could be
86    used as features in further developing SARS-CoV-2 related biomarkers (Figure 1). One of the
87    distinguishing characteristics of SARS-CoV-2 infection is the wide range of potential exposure outcomes,
88    from transient, asymptomatic infection to severe disease requiring hospitalization and intensive care.
89    While there are high quality biomarkers for detecting active SARS-CoV-2 infection via viral RNA qPCR
90    (Nalla et al., 2020) and prior exposure via antibody ELISA (Espejo et al., 2020), additional biomarkers
91    capable of predicting susceptibility to symptomatic infection or severe disease could help guide clinical
92    care and public health policy. Several studies have begun to describe the cellular adaptive immune
93    responses that are elicited by SARS-CoV-2 infection and how they correlate with disease severity (Grifoni
94    et al., 2020; Le Bert et al., 2020; McMahan et al., 2020; Tan et al., 2021; Wang et al., 2020; Weiskopf et
95    al., 2020). These and other studies have also established that 20-50% of unexposed individuals have T
96    cell responses to SARS-CoV-2, raising the hypothesis that prior exposure to "common-cold"
97    coronaviruses or other viral antigens may shape the response to SARS-CoV-2 infection (Sette and Crotty,
98    2020; Welsh and Selin, 2002). T cells likely play an integral role in SARS-CoV-2 pathogenesis and may
99    be an important target for biomarker development. For instance, a TCR biomarker of pre-existing SARS-
100   CoV-2 responses could help predict the course of infection. A T cell-based biomarker might also play a
101   role in vaccine development, for which immunological surrogates of vaccine-induced protection or
102   response durability are highly valued. Most published studies have had limited ability to determine
103   quantitative immunodominance hierarchies, relying on pooled peptide assays, due to the large size of the
104   SARS-CoV-2 proteome and HLA diversity; direct repertoire measurement tied to identified epitopes is a
105   complementary approach to resolve the associated magnitude and specificity of the total T cell response.

106       One recent study to elucidate the role of cellular immune responses in acute SARS-CoV-2
107   infection examined the T cell receptor repertoires of patients diagnosed with COVID-19 disease.
108   Researchers used an assay based on antigen stimulation and flow cytometric sorting of activated CD8+ T
109   cells to sequence SARS-CoV-2 peptide-associated TCR β-chains; the assay is called "multiplex
110   identification of T-cell receptor antigen specificity" or MIRA (Klinger et al., 2015). Data from these
111   experiments were released publicly in July 2020 by Adaptive Biotechnologies and Microsoft as part of
112   "immuneRACE" and their efforts to stimulate science on COVID-19 (Nolan et al., 2020; Snyder et al.,
113   2020). The MIRA antigen enrichment assays identified 269 sets of TCR β-chains associated with CD8+ T
114   cells activated by exposure to SARS-CoV-2 peptides, with TCR sets ranging in size from 1 - 16,607 TCRs
115   (Table S1). The deposited immuneRACE datasets also included bulk TCR β-chain repertoires from 694
116   patients within 0-30 days of COVID-19 diagnosis. To demonstrate potential uses of our new analytical

117   tools for TCR repertoire analysis and to accelerate understanding of the cellular responses to SARS-CoV-
118   2 infection, we present analyses of these data with a focus on an integration of the peptide-associated
119   MIRA TCR repertoires with bulk repertoires from four COVID-19 observational studies that enrolled
120   patients with diversity in age and geography (Alabama, USA n = 374; Madrid, Spain, n=117; Pavia, Italy,
121   n=125; Washington, USA, n=78).

122   

123   **FRAMEWORK**

124   

125   *Experimental antigen-enrichment allows discovery of TCRs with biochemically similar neighbors*

126   

127   Searching for identical TCRs within a repertoire - arising either from clonal expansion or
128   convergent nucleotide encoding of amino acids in the CDR3 - is a common strategy for identifying
129   functionally important receptors. However, in the absence of experimental enrichment procedures,
130   observing T cells with the same amino acid TCR sequence in a bulk sample is rare. For example, in
131   10,000 β-chain TCRs from an umbilical cord blood sample, less than 1% of TCR amino acid sequences
132   were observed more than once, inclusive of possible clonal expansions (Figure 2A). By contrast, a
133   valuable feature of antigen-enriched repertoires is the presence of multiple T cells with identical or highly
134   similar TCR amino acid sequences (Figure 2A). For instance, 45% of amino acid TCR sequences were
135   observed more than once (excluding clonal expansions) in a set of influenza M1(GILGFVFTL)-A*02:01
136   peptide-MHC tetramer sorted sub-repertoires from 15 subjects (Dash et al., 2017). Enrichment was
137   evident compared to cord blood for additional peptide-MHC tetramer sorted sub-repertoires obtained from
138   VDJdb (Shugay et al., 2018), though the proportion of TCRs with an identical or similar TCR in each set
139   was heterogeneous.
140   We investigated the degree to which the MIRA enrichment strategy employed by Nolan et al.
141   (2020) identified TCRs with identical or similar amino acid sequences. In general, across multiple MIRA
142   TCR β-chain antigen-enriched repertoires, the proportion of amino acid TCR sequences observed more
143   than once was generally lower than in the tetramer-enriched repertoires and varied considerably across
144   the sets; some MIRA sets resembled tetramer-sorted sub-repertoires (Figure 2B; see MIRA133), while
145   others were more similar to unenriched repertoires (Figure 2B; see MIRA90). The increased diversity in
146   MIRA-enriched TCR sets versus tetramer-enriched TCR sets may, in part, be explained by: (i) peptides
147   being presented by the full complement of the native host's MHC molecules compared to a single defined
148   peptide-MHC complex, (ii) recruitment of lower affinity receptors, or (iii) non-specific "bystander" activation
149   in the MIRA stimulation assay.

150   

151   *TCR biochemical neighborhood density is heterogeneous in antigen-enriched repertoires*

152   

153   We next investigated the proportion of unique TCRs with at least one biochemically similar
154   neighbor among TCRs with the same putative antigen specificity. We and others have shown that a
155   single peptide-MHC epitope is often recognized by many distinct TCRs with closely related amino acid
156   sequences (Dash et al., 2017); in fact, detection of such clusters in bulk-sequenced repertoires is the
157   basis of several existing tools: GLIPH (Glanville et al., 2017; Huang et al., 2020), ALICE (Pogorelyy et al.,
158   2019) and TCRNET (Ritvo et al., 2018). Therefore, to better understand new large-scale antigen-enriched
159   datasets, like the SARS-CoV-2 MIRA data, we evaluated the TCR biochemical neighborhoods, defined

160    for each TCR as the set of similar TCRs whose sequence divergence is within a specified radius. The

161    radius was measured using a position weighted, multi-CDR TCR distance metric. Briefly, differences in

162    the amino-acid sequences of the CDRs are totaled based on number of gaps (-4) and their BLOSUM62

163    substitution penalties (ranging from 0 to -4) with 3-fold weighting on CDR3 substitutions (see Methods for

164    details of *tcrdist3* re-implementation of TCRdist); a one amino-acid mismatch in the CDR3 results in a

165    maximal distance of 12 TCRdist units (tdus). As the radius about a TCR centroid expands, the number of

166    TCRs it encompasses naturally increases; the rate of increase is more rapid in the antigen-enriched

167    repertoires compared to the unenriched repertoires (Figure 2).

168        To better understand the relationship between the TCR distance radius and the density of

169    proximal TCRs, we constructed empirical cumulative distribution functions (ECDFs) for each unique TCR

170    found within a repertoire (Figure 3). The ECDF for each unique TCR (one line in Figure 3) shows the

171    proportion of all TCRs within the indicated radius; those with sparse neighborhoods appear as lines that

172    remain flat and do not increase along the *y*-axis even as the search radius expands. Moreover, the

173    proportion of TCRs with sparse or empty neighborhoods (ECDF proportion < 0.001) is indicated by the

174    height of the gray area plotted below the ECDF (Figure 3). We observed the highest density

175    neighborhoods within repertoires that were sorted based on peptide-MHC tetramer binding. For instance,

176    with the influenza M1(GILGFVFTL)-A*02:01 tetramer-enriched repertoire from 15 subjects, we observed

177    that many TCRs were concentrated in dense neighborhoods, which included as much as 30% of the

178    other influenza M1-recognizing TCRs within a radius of 12 tdus (Figure 3A). Notably there were also

179    many TCRs with empty or sparse neighborhoods using a radius of 12 tdus (111/247, 44%) or 24 tdus

180    (83/247, 34%). Based on previous work (Dash et al., 2017), we assume that the majority of these

181    tetramer-sorted CD8+ T cells without many close proximity neighbors do indeed bind the influenza

182    M1:A*02:01 tetramer. This suggests that TCRs within sparse neighborhoods represent less common

183    modes of antigen recognition and highlights the broad heterogeneity of neighborhood densities even

184    among TCRs recognizing a single pMHC.

185        Neighbor densities for individual TCRs within MIRA identified antigen-enriched repertoires were

186    highly heterogeneous. Densities for an illustrative MIRA set are shown in Figure 4 (MIRA55:ORF1ab;

187    1316:1330 (amino acid); peptide ALRKVPTDNYITTY). Within this antigen-enriched repertoire, at 24 tdus

188    8.9% (44/497) of TCR neighborhoods included >10% of the other antigen-activated CD8+ TCRs (Figure

189    4A). As expected, TCR neighborhoods in the umbilical cord blood repertoire were sparser (Figure 4B);

190    the densest neighborhood included only 0.13% of the repertoire at 24 tdus. We also noted that TCRs with

191    empty neighborhoods tended to have longer CDR3 loops (Figure 4C). This is consistent with

192    mathematical modeling approaches that show that TCRs with longer CDR3 loops have a lower

193    generation probability ($P_{gen}$) during genomic recombination of the TCR locus (Marcou et al., 2018;

194    Murugan et al., 2012; Sethna et al., 2019). Absent strong selection for antigen recognition, TCRs with a

195    low generation probability are thus likely to have a less dense biochemical neighborhood. Together, these

196    observations suggest that biochemical neighborhood density is highly heterogeneous among TCRs and

197    that it may depend on mechanisms of antigen-recognition as well as receptor V(D)J recombination biases

198    (Thomas and Crawford, 2019).

199

200

*Meta-clonotype radius can be tuned to balance a biomarker's sensitivity and specificity*

The utility of a TCR-based biomarker depends on the antigen-specificity of the TCRs. Therefore, a key constraint on distance-based clustering is the presence of similar TCR sequences that may lack the ability to recognize the target antigen. To be useful, a meta-clonotype definition should be broad enough to capture multiple biochemically similar TCRs with shared antigen-recognition, but not excessively broad as to include a high proportion of non-specific TCRs, which might be found in unenriched background repertoires that are largely antigen-naïve. Because the density of neighborhoods around TCRs are heterogeneous, we hypothesize that the optimal radius defining a meta-clonotype may differ for each TCR. To find the ideal radius we proposed comparing the relative density of a radius-defined neighborhood in an antigen-enriched sub-repertoire (Figure 4A) to the density of the radius-defined neighborhood in an unenriched background repertoire (Figure 4B, 4C). This is similar to previous approaches taken by tools like ALICE and TCRNET, except that we employ a biochemically informed distance measure (TCRdist) and adjust the radius around each TCR to balance the antigen-enriched and unenriched neighborhood densities. The radius around each TCR defines a meta-clonotype that can be used to search for and quantify the abundance of conformant sequences in bulk repertoires (Figure 1A, 1B). For each TCR, its radius-defined meta-clonotype is more abundant within a repertoire and more prevalent in a population than the exact clonotype; for example, TCR meta-clonotypes formed from the MIRA55:ORF1ab TCR set were detected in 3 to 12 (median 6) of 15 HLA-A*01 participants in the MIRA cohort, despite 34 of the 46 centroid clonotype TCRs being private (i.e., found in only 1 of 15 HLA-A*01 participants). (Figure S1).

An ideal radius-defined meta-clonotype would include a high density of TCRs in antigen-experienced individuals indicative of shared antigen specificity, yet a low density of TCRs among an antigen-naïve background. We demonstrate this approach for selecting an optimal radius for TCRs in the MIRA55:ORF1ab dataset, which includes TCRs from 15 COVID-19 diagnosed subjects (see Methods for details about MIRA and the immuneRACE dataset). First, an ECDF is constructed for each centroid TCR showing the relationship between the meta-clonotype radius and its "sensitivity": its inclusion of similar antigen-recognizing TCRs, approximated by the proportion of TCRs in the antigen-enriched MIRA set that are within the centroid's radius (Figure 4A). Next, an ECDF is constructed for each TCR showing the relationship between the meta-clonotype radius and its "specificity": its exclusion of TCRs with divergent antigen-recognition; this is assessed by computing the false-positive rate (one minus specificity) which is approximated by the proportion of TCRs in an unenriched background repertoire within the centroid's radius (Figure 4B). Generating an appropriate set of unenriched background TCRs is important; for each set of antigen associated TCRs discovered by MIRA, we created a two part background. One part consisted of 100,000 synthetic TCRs whose TRBV- and TRBJ-gene frequencies matched those in the antigen-enriched repertoire; TCRs were generated using the software OLGA (Marcou et al., 2018; Sethna et al., 2019). The other part consisted of 100,000 umbilical cord blood TCRs sampled from 8 subjects (Britanova et al., 2017). This composition balanced denser sampling of sequences near the candidate meta-clonotype centroids with broad sampling of TCRs from an antigen-naïve repertoire. Importantly, we adjusted for the biased sampling by using the TRBV- and TRBJ-gene frequencies observed in the cord blood data (see Methods for details about inverse probability weighting adjustment). Using this approach, we are able to estimate the abundance of TCRs similar to a centroid TCR in an unenriched background repertoire of effectively ~1,000,000 TCRs, using a comparatively modest background dataset of 200,000

244  TCRs. While this may underestimate the true specificity since some of the neighborhood TCRs in the
245  unenriched background repertoire may in fact recognize the antigen of interest, this measure is useful for
246  prioritizing neighborhoods and selecting a radius for each neighborhood that balances sensitivity and
247  specificity.

248      We find that the neighborhoods around TCR centroids with higher probabilities of generation
249  consistently span a larger proportion of unenriched background TCRs across a range of radii, suggesting
250  that a smaller radius may be desirable for forming meta-clonotypes from high $P_{gen}$ TCRs. With a large
251  radius, most TCR centroids had high sensitivity and low specificity, indicated by the meta-clonotypes
252  including both a high proportion of TCRs from the antigen-enriched and unenriched repertoires. Some
253  TCRs had low sensitivity and specificity even at a radius of 24 tdus, indicative of a low $P_{gen}$ or "snowflake"
254  TCR: a seemingly unique TCR in both the antigen-enriched and unenriched repertoires. However, radius-
255  defined neighborhoods around many TCRs in the MIRA55:ORF1ab repertoire included 1 - 10% of the
256  antigen-enriched repertoire (5-50 clonotypes) with a radius that included fewer than 0.0001% of TCRs
257  (equivalent to 1 out of $10^6$) in the unenriched background repertoire, demonstrating a level of sensitivity
258  and specificity that would be favorable for development of a TCR biomarker (Figure 4C, one example
259  meta-clonotype).

260

261  **RESULTS**

262

263  *Engineering meta-clonotype features for SARS-CoV-2*

264

265      The MIRA antigen enrichment assays identified 269 sets of TCR β-chains associated with
266  recognition of a SARS-CoV-2 antigen using CD8+ T cell enriched PBMC samples from 62 COVID-19
267  diagnosed patients. Of these, 252 included at least 6 unique TCRs from ≥ 2 individuals, which we refer to
268  as MIRA1 - MIRA252 based on the number of sequences observed, in descending order (Table S2).
269  From the MIRA enriched repertoires, all TCR clonotypes (defined by identical TRBV gene and CDR3 at
270  the amino acid level) were initially considered as candidate centroids; only 2.7% of the clonotypes were
271  found in more than one MIRA participant. For each candidate TCR, a meta-clonotype was engineered by
272  selecting the maximum radius that limited the estimated number of neighboring TCRs in a bulk
273  unenriched repertoire to less than 1 in $10^6$, estimated using an inverse probability weighted antigen-naïve
274  background repertoire (see Methods). We then ranked the meta-clonotypes by their sensitivity
275  approximated as the proportion of a centroid's MIRA-enriched repertoire spanned by the search radius
276  (diagrammed in Figure 1). Lower-ranked meta-clonotypes were eliminated if all included sequences were
277  completely encompassed by a higher-ranked meta-clonotype; while this reduced redundancy, some
278  overlap remained among meta-clonotypes. We further required that meta-clonotypes be public, including
279  sequences from at least two subjects in the MIRA cohort. We found that 97 of the 252 MIRA sets (Table
280  S6) had sufficiently similar TCRs observed in multiple subjects allowing formation of public meta-
281  clonotypes. From 91,122 TCR β-clonotypes across these 97 MIRA sets -- targeting antigens in ORF1ab
282  (n=35), S (n=27), N (n=10), M (n=7), ORF3a (n=7), ORF7a (n=4), E (n=2), ORF8 (n=2), ORF6 (n=1),
283  ORF7b (n=1), and ORF10 (n=1) -- we engineered 4548 public meta-clonotypes, which spanned 15%
284  (13,949/91,122) of the original TCR sequences (Table S6). The proportion of MIRA-enriched TCRs
285  spanned by the meta-clonotypes ranged widely from <1% in MIRA25 to 63% in MIRA7, reflecting broad
286  heterogeneity in the diversity of TCRs inferred as activated by each peptide in the assay.

287    As an example, the MIRA repertoire MIRA55 ORF1ab (TCRs associated with stimulation
288    peptides ALRKVPTDNYITTY or KVPTDNYITTY) included 449 TCR clonotypes from 15 individuals. From
289    the 449 potential centroids, we defined 40 public meta-clonotypes. Among these features, the radii
290    ranged from 10-36 tdus (median 22 tdus), and the publicity - the number of unique subjects spanned by
291    the meta-clonotype - ranged from 3 to 12 individuals (median 6). Meta-clonotype summary statistics for
292    other enriched repertoires are provided in the Supplemental Materials (Table S6). The result was a set of
293    non-redundant, public meta-clonotypes (Table S7, S8) that could be used to search for and quantify
294    putative SARS-CoV-2-specific TCRs in bulk repertoires. In addition to the radius-defined meta-clonotypes
295    (RADIUS), we also developed a modified approach that additionally enforced a sequence motif-constraint
296    (RADIUS + MOTIF). The constraint further limited sequence divergence in highly conserved positions of
297    the CDR3, requiring that candidate bulk TCRs match specific amino acids found in the meta-clonotype
298    CDR3s to be counted as part of the neighborhood (see Figure 1 and Methods).
299
300    *Evidence of HLA-restriction in SARS-CoV-2 antigen-enriched sub repertoires*
301
302    Given the integral role of HLA class I molecules in antigen presentation and TCR repertoire
303    selection (DeWitt, 2018), we further focused on the 17 of the 269 MIRA sets that showed strong evidence
304    of HLA-A or HLA-B restriction based on two criteria: (i) computational prediction of HLA binding to the
305    SARS-CoV-2 stimulation peptides, and (ii) enrichment of an HLA among participants contributing MIRA
306    TCRs. With each set of the MIRA TCRs and the associated SARS-CoV-2 peptides we used HLA binding
307    predictions (NetMHCpan4.0) to identify the class I HLA alleles that were predicted to bind with strong
308    (IC50<50 nM) or weak (50 nm< IC50 <500 nM) affinity to any of the 8, 9, 10, or 11-mers derived from the
309    stimulation peptides (Tables S2, S3). For instance, the peptides associated with MIRA55 TCRs (ORF1ab
310    amino acid positions 1316:1330) are predicted to preferentially bind A*01 (IC50 21 nM), B*15 (IC50 120
311    nM), and B*35 (IC50 32 nM), and peptides associated with MIRA51 TCRs (nucleocapsid amino acid
312    positions 359:370) are predicted to bind A*03 (IC50 19 nM), A*11 (IC50 8 nM), and A*68 (IC50 9 nM).
313    Of the COVID-19 patient samples screened using the MIRA assay, HLA genotypes were
314    available for 47 of 62 patients and only a subset of patients contributed TCRs to each of the MIRA sets.
315    As a second indicator of HLA restriction, we tested whether the subgroup of patients contributing TCRs to
316    each MIRA set was enriched with individuals expressing specific HLA class I alleles (2-digit resolution)
317    (Table S5). We found that for 17 of the MIRA sets, the patients contributing TCRs were significantly
318    enriched for at least one HLA-A or HLA-B allele (Fisher's exact test p<0.001). In one case, all 13 A*01-
319    positive, and only 2 of 34 A*01-negative, patients contributed to the MIRA55 TCR set (p=1e-7); as noted
320    above, A*01 was also strongly predicted by NetMHCpan4.0 to bind the MIRA55 ORF1ab peptides.
321    Similar patterns of enrichment and predicted binding were seen with A*01 expressing individuals and
322    recognition of MIRA1:ORF1ab (HTTDPSFLGRY, p=1.9e-7) and MIRA45:ORF3a (SYFTSDYYQ, p=1.9e-
323    7). Similarly, for the other 16 MIRA sets examined, we found consistent evidence between peptide
324    binding prediction (IC50 < 500 nM) and MIRA participant genotype enrichment (fisher's exact test p <
325    0.001) to support HLA-restriction (Table S5).
326
327

*HLA-associated abundance of SARS-CoV-2 meta-clonotypes in bulk repertoires of COVID-19 patients*

We focused confirmatory analyses on TCR meta-clonotypes derived from the 17 SARS-CoV-2 MIRA-identified TCR sets that showed strongest evidence of HLA restriction by HLA-A or HLA-B alleles. We hypothesized that in an independent cohort of COVID-19 patients, the abundance of TCRs matching each meta-clonotype would be greater in patients expressing the restricting HLA allele. To test this hypothesis, we compared three TCR-based feature sets: (i) radius-defined meta-clonotypes, (RADIUS), (ii) radius and motif-defined meta-clonotypes (RADIUS+MOTIF) and (iii) centroid clonotypes alone, using TRBV-CDR3 amino acid matching (EXACT). Using the features in each set we screened TCRs from the bulk TCR β-chain repertoires of 694 COVID-19 patients whose repertoires were publicly released as part of the immuneRACE datasets (see Methods for details); these patients were not part of the smaller cohort that contributed samples for TCR identification in MIRA experiments. Testing the HLA restriction hypothesis required having the HLA genotype of each individual, which was not provided in the dataset. To overcome this, we inferred each participant's HLA genotype with a classifier that was based on previously published HLA-associated TCR β-chain sequences (DeWitt et al., 2018) and their abundance in each patient's repertoire (see Methods for details). MIRA TCRs were not used to assign HLA-types to the 694 COVID-19 patients. We then used a beta-binomial counts regression model (Rytlewski et al., 2019) with each TCR feature to test for an association of feature abundance with presence of the restricting allele in the participant's HLA genotype, controlling for participant age, sex, and days since COVID-19 diagnosis.

The models revealed that there were radius-defined meta-clonotypes with a strong positive and statistically significant association (FDR < 0.01) for 11 of the 17 HLA-restricted-MIRA sets that were evaluated (Figure 5A, Table S7); the significant HLA regression odds ratios ranged from 1.4 to 40 (median 4.9), indicating log-fold differences in meta-clonotype frequency between patients with and without the HLA genotype. Across all MIRA sets, an HLA-association (FDR < 0.01) was detected for 51.5% (943/1831) and 59.7% (830/1831) of the meta-clonotypes using the RADIUS or RADIUS+MOTIF definitions, respectively. In comparison, an HLA-association (FDR < 0.01) was detected for fewer than 3.7% (69/1831) of EXACT centroid features, largely because the specific TRBV gene and CDR3 sequences discovered in the MIRA experiments were infrequently observed in unenriched bulk samples (Figure 5B). When detectable, the abundance of centroid TCRs in bulk repertoires tended to be positively associated with expression of the restricting HLA allele, as hypothesized. However, in most cases, the associated false discovery rate-adjusted q-value of these associations were orders of magnitude larger (i.e., less statistically significant) than those obtained from using the engineered RADIUS or RADIUS+MOTIF feature with the same clonotype as a centroid (Figure 6B). The improved performance of meta-clonotypes as query features is particularly evident when testing for HLA-associated enrichment of TCRs recognizing immunodominant MIRA1 A*01, MIRA48 A*02, MIRA51 A*03, MIRA53 A*24, and MIRA55 A*01 (Figure 6). Moreover, the regression models with meta-clonotypes also revealed possible negative associations between TCR abundance and participant age and positive associations with sample collection more than two days post COVID-19 diagnosis (Figure 6A).

368     *Comparison to k-mer based CDR3 features*

369

370           Alternative methods exist for generating public TCR features from clustered clonotypes. One

371   strategy is to identify clusters of TCRs that are each uniquely enriched with a short CDR3 k-mer, as

372   implemented in GLIPH2 (Huang et al., 2020); this approach is well suited for identifying CDR3 k-mers

373   associated with antigenic selection across bulk repertoires when knowledge of the specific antigens is

374   unavailable (Chiou et al., 2021). To evaluate the similarities and differences of using this approach to

375   generate public TCR features, compared with TCR distance-based meta-clonotypes, we applied tcrdist3

376   and GLIPH2 to 16 HLA-restricted MIRA sets (Figure 7; see Methods for details). Both methods identified

377   public molecular patterns from MIRA TCRs (Figure S2) that were strongly HLA-associated in the large

378   independent cohort of COVID-19 diagnosed patients (Figure 7). For this non-standard application of

379   GLIPH2, we found that specificity groups based on global CDR3 k-mers (e.g., 'SFRTD.YE') tended to be

380   more consistently HLA-associated than specificity groups based on local k-mers (e.g., 'FRTD'). Compared

381   to the GLIPH2 specificity groups based on global CDR3 kmers, meta-clonotypes tended to show similar

382   or more evidence of HLA-association (i.e., smaller FDR values) (Figure 7). MIRA55:ORF1ab is an

383   illustrative example; both the tcrdist3 meta-clonotypes GLIPH2 TCR groups were more strongly

384   associated with the predicted A*01:01 HLA-restriction than exact clonotypes, supporting the general

385   applicability of using antigen-enriched repertoires to create public features from otherwise private antigen-

386   recognizing TCRs. Inspection of the meta-clonotypes and GLIPH2 groups showed that they were often

387   overlapping, with meta-clonotypes subsuming multiple GLIPH2 groups. For example, A*01-associated

388   meta-clonotype TRBV5-5*01+S.G[QE]G[AS]F[ST]DTQ (p-value 1E-12) fully overlaps several A*01-

389   associated GLIPH2 patterns including S.GQGAFTDT (p-value 1E-12), QGAF (p-value 1E-11), and

390   SLG.GAFTDT (p-value 1E-6). Similarly, the A*01-associated meta-clonotype

391   TRBV28*01+S[RLMF][RK][ST][ND].YEQ (p-value 1E-13) covers 21 global GLIPH motifs including

392   SFRTD.YE (p-value 1E-10), SLRTD.YE (p-value 1E-7), and SF.TDSYE (p-value 1E-4) (Table S9). These

393   observations suggest that the motif-constraints of the meta-clonotypes were able to match a broader set

394   of antigen-specific CDR3s compared to any one GLIPH2 specificity pattern, which may have helped

395   boost detection sensitivity in the COVID-19 repertoires.

396

397   **DISCUSSION**

398

399           Given the extent of TCR diversity, only antigen-specific TCRs with high probability of generation

400   ($P_{gen}$) are likely to be detected reliably across individuals (Figure S3). While public, high-$P_{gen}$ TCRs may

401   sometimes be available for detecting a prior antigen-exposure, to more fully understand the population-

402   level dynamics of complex polyclonal T-cell responses across a gradient of generation probabilities, it is

403   critical to develop methods for finding public meta-clonotypes that capture otherwise private TCRs (Figure

404   S3). We developed a novel framework, integrating antigen-enriched repertoires with efficiently sampled

405   unenriched background repertoires, to engineer meta-clonotypes that balance the need for sufficiently

406   public features with the need to maintain antigen specificity. The output of the analysis framework (Figure

407   1A) is a set of meta-clonotypes, each represented by a (i) centroid, (ii) radius, and (iii) optionally, a CDR3

408   motif-pattern, that can be used to rapidly search bulk repertoires for similar TCRs that likely share a

409   cognate antigen. To demonstrate this analytical framework, we analyzed publicly available sets of

410   antigen-enriched TCR β-chain sequences that putatively recognize SARS-CoV-2 peptides (Nolan et al.,

411 2020). From these, we generated 4548 TCR radius-defined public meta-clonotypes that could be used to
412 further investigate CD8+ T cell response to SARS-CoV-2 (Tables S7, S8).

413 To evaluate the potential relevance of radius-defined meta-clonotypes we focused on those with
414 the strongest evidence of HLA restriction (Table S7, n=1831). We reasoned that we could compare the
415 abundance of these meta-clonotypes in COVID-19 patients with and without the restricting HLA allele,
416 where a significant positive association of abundance with expression of the restricting allele would
417 provide confirmatory evidence both of the SARS-CoV-2 specificity of the meta-clonotype and its HLA
418 restriction (Figure 1B). Overall, we found confirmation of HLA-restriction of meta-clonotype abundance for
419 a majority of the MIRA sets we analyzed (11/17) and for 59% of meta-clonotypes tested using the
420 RADIUS+MOTIF approach. There are several plausible explanations for the remaining meta-clonotypes
421 that were not significantly HLA-restricted in this study. One possibility is that meta-clonotype definitions
422 are not sufficiently specific for the target antigen; the radius is optimized for specificity, but not all amino
423 acid substitutions accommodated within the radius are guaranteed to preserve antigen recognition, and
424 while the motif constraint increases specificity, it's likely that meta-clonotype definitions could be further
425 refined with more antigen enriched TCR data and enhanced motif refinement methods. Also, sub-
426 dominant SARS-CoV-2 epitopes may not be uniformly recognized, even among participants that share
427 the required HLA genotype, which weakens the signal of HLA restriction detectable by regression
428 analysis. A subset of GLIPH2 k-mer patterns were similar in their success at identifying groups of TCRs
429 that confirmed the HLA restriction; it appeared that meta-clonotypes were generally more sensitive at the
430 task, possibly afforded by non-conserved and multiple degenerate positions in the motif and lack of a
431 constraint on the length of the CDR3, both of which enabled single meta-clonotypes to cover multiple
432 GLIPH2 groups.

433 Recently, Snyder et al. (2020) analyzed 1521 bulk TCR β-chain repertoires from COVID-19
434 patients in the immuneRACE dataset and an additional 3500 (not yet publicly available) repertoires from
435 healthy controls to identify public TCR β-chains that could be used to identify SARS-COV-2 infected
436 individuals with high sensitivity and specificity. Their results show that with sufficient data it is possible to
437 engineer highly performant TCR biomarkers of antigen exposure from exact clonotypes. We show that by
438 leveraging antigen-enriched TCR repertoires it is possible to engineer radius-defined TCR meta-
439 clonotypes from a relatively small group of COVID-19 diagnosed individuals (n=62; HLA-typed n=47) that
440 are frequently detected in much larger independent cohorts. We propose that meta-clonotypes constitute
441 a set of potential features that could be leveraged in developing TCR-based clinical biomarkers that go
442 beyond detection of infection or exposure. For example, biomarkers predictive of infection, disease
443 severity or vaccine protection may all require different TCR features. Statistical and machine learning
444 tools could be employed to identify the meta-clonotypes and meta-clonotype combinations that carry the
445 relevant clinical signal. Much like any biomarker study, to establish a TCR-based predictor of a particular
446 outcome, the features must be measured among a sufficiently large cohort of individuals, with a sufficient
447 mix of outcomes.

448 Though demonstrating HLA restriction of the SARS-CoV-2 meta-clonotypes establish their
449 potential utility, it also highlighted how HLA diversity could be a major hurdle to biomarker development.
450 The sensitivity of a TCR-based biomarker in a diverse population may depend on combining meta-
451 clonotypes with diverse HLA restrictions since individuals with different HLA genotypes often target
452 different epitopes using divergent TCRs. Our analysis shows that having HLA genotype information for
453 TCR repertoire analysis can be critical to interpreting results. The simple HLA classifier we developed

454  suggests that in the near future it may be possible to infer high-resolution HLA genotype from bulk TCR
455  repertoires, but until then it is valuable to have sequenced-based HLA genotyping. In the absence of HLA
456  genotype information, it may still be feasible to generate informative TCR meta-clonotypes. For example,
457  a poly-antigenic TCR-enrichment strategy (i.e., peptide pools or whole-proteins) could help generate
458  meta-clonotypes that broadly cover HLA diversity if the sample donors are racially, ethnically and
459  geographically representative of the ultimate target population. For these reasons, donor unrestricted T
460  cells and their receptors (e.g., MAITs, γδ T cells) may also be good targets for TCR biomarker
461  development.

462  To enable TCR biomarker development and innovative extensions of distance-based immune
463  repertoire analysis, we developed *tcrdist3*, which provides open-source
464  (https://github.com/kmayerb/tcrdist3), documented (https://tcrdist3.readthedocs.io) computational building
465  blocks for a wide array of TCR repertoire workflows in Python3. The software is highly flexible, allowing
466  for: (i) customization of the distance metric with position and CDR-specific weights and amino acid
467  substitution matrices, (ii) inclusion of CDRs beyond the CDR3, (iii) clustering based on single-chain or
468  paired-chain data for α/β or γ/δ TCRs, and (iv) use of default as well as user-provided TCR repertoires as
469  background for controlling meta-clonotype specificity (e.g., users may want to use HLA genotype-
470  matched, or age-matched backgrounds). *tcrdist3* makes efficient use of available CPU and memory
471  resources; as a reference, identification of meta-clonotypes from the MIRA55:ORF1ab dataset (n=479
472  TCRs) was completed in less than 5 minutes using 2 CPU and < 4 GB of memory including distance
473  computation and radius optimization. Quantification of the identified meta-clonotypes (n=40) in 694 bulk
474  TCR β-chain repertoires, ranging in size from 10,395 to 1,038,012 in-frame clones (~5 billion total
475  pairwise comparisons) could be completed in less than 2 hours using 2 CPU and < 6 GB memory. The
476  package also can generate multiple types of publication-ready figures (e.g., background-adjusted CDR3
477  sequence logos, V/J-gene usage chord diagrams, and annotated TCR dendrograms). The continued
478  maturation of multiple adaptive immune receptor repertoire sequencing technologies will open
479  possibilities for basic immunology and clinical applications, and *tcrdist3* provides a flexible tool that
480  researchers can use to integrate the data sources needed to detect and quantify antigen-specific TCR
481  features.

482

483  **METHODS**

484

485  *TCR Data: immuneRACE datasets and MIRA assay*

486

487  The study utilized two primary sources of TCR data (Nolan et al. 2020; Snyder et al. 2020). The
488  first data source was a table of TCR β-chains amplified from CD8+ T cells activated after exposure to a
489  pool of SARS-CoV-2 peptides, using a Multiplex Identification of Receptor Antigen (MIRA) (Klinger et al.
490  2015); data was accessed Jul 21, 2020 and labeled "ImmuneCODE-MIRA-Release002". The samples
491  used for the MIRA analysis included samples from 62 individuals diagnosed (3 acute, 1 non-acute, 58
492  convalescent) with COVID-19, of whom 47 (3 acute, 44 convalescent) were HLA-genotyped in the
493  ImmuneCODE-MIRA-Release002 *subject-metadata.csv* file. We also used TCRs evaluated by MIRA from
494  26 COVID-19-negative control subjects that were part of ImmuneCODE-MIRA-Release002. We analyzed
495  the 252 MIRA sets with at least 6 unique TCRs, referred to as MIRA1-MIRA252 in rank order by their size
496  (Table S2); each "MIRA set" included antigen-associated TCRs across all assayed individuals. Adaptive

497 Biotechnologies also made publicly available bulk unenriched TCR β-chain repertoires from COVID-19

498 patients participating in a collaborative immuneRACE network of international clinical trials. We selected

499 repertoires from 694 individuals where meta-data was available indicating that the sample was collected

500 from 0 to 30 days from the time of diagnosis. (COVID-19-DLS (Alabama, USA n = 374); COVID-19-

501 HUniv12Oct (Madrid, Spain n = 117); COVID-19-NIH/NIAID (Pavia, Italy n=125) + COVID-19-ISB

502 (Washington, USA n = 78). The sampling depth of these repertoires varied from 15,626-1,220,991

503 productive templates (median 208,709) and 10,395-1,038,012 productive rearrangements (median

504 113,716). We did not use bulk samples from the COVID-19-ADAPTIVE dataset as the average age was

505 substantially lower than other immuneRACE populations and to avoid possible overlap with individuals

506 that contributed samples to the MIRA experiments.

507

508 *HLA genotype inferences*

509

510 No publicly available HLA genotyping was available for the 694 bulk unenriched immuneRACE T

511 cell repertoires (Nolan et al. 2020). Before considering SARS-CoV-2 specific features, we inferred the

512 HLA genotypes of these participants based on their TCR repertoires. Predictions were based on

513 previously published HLA-associated TCR β-chain sequences (DeWitt et al., 2018) and their detection in

514 each repertoire. Briefly, a weight-of-evidence classifier for each HLA loci was computed as follows: For

515 each sample and for each common allele, the number of detected HLA-diagnostic TCR β-chains was

516 divided by the total possible number of HLA-diagnostic TCR β-chains. The weights were normalized as a

517 probability vector and the two highest HLA-allele probabilities (if the probability was larger than 0.2) were

518 assigned to each repertoire; homozygosity was inferred if only one allele had probability > 0.2. The

519 sensitivity and specificity of this simple classifier for each allele prediction were assessed using 550 HLA-

520 typed bulk repertoires (Emerson et al., 2017). Sensitivities for common HLA-A alleles A*01:01, A*02:01,

521 A*03:01, A*24:02, and A*11:01 were 0.96, 0.91, 0.90. 0.84, 0.94, respectively. Specificity for major HLA-A

522 alleles was between 0.97-1.0. Inference of the HLA genotype of most participants was deemed sufficient

523 in the absence of direct HLA genotyping.

524

525 *Peptide-HLA binding prediction*

526

527 HLA binding affinities of peptides used in the MIRA stimulation assay were computationally

528 predicted using NetMHCpan4.0 (Jurtz et al., 2017). Specifically, the affinities of all 8, 9, 10 and 11mer

529 peptides derived from the stimulation peptides were computed with each of the class I HLA alleles

530 expressed by participants in the MIRA cohort (n=47). From this data we derived 2-digit HLA binding

531 predictions (e.g., A*02) for each MIRA set by pooling the predictions for all the 4-digit HLA variants (e.g.

532 A*02:01, A*02:02) across all the derivative peptides and selecting the lowest IC50 (strongest affinity).

533 Predictions with IC50 < 50 nM were considered strong binders and IC50 < 500 nM were considered weak

534 binders (Table S3, Table S4).

535

536 *TCR distances*

537

538 Weighted multi-CDR distances between TCRs were computed using *tcrdist3*, an open-source

539 Python3 package for TCR repertoire analysis and visualization, using the procedure first described in

540    (Dash et al., 2017). The package has been expanded to accommodate γδ TCRs; it has also been re-

541    coded to increase CPU efficiency using *numba*, a high-performance just-in-time compiler. A numba-

542    coded edit/Levenshtein distance is also included for comparison, with the flexibility to accommodate novel

543    TCR metrics as they are developed.

544          Briefly, the distance metric in this study is based on comparing TCR β-chain sequences. The

545    *tcrdist3* default settings compare TCRs at the CDR1, CDR2, and CDR2.5 and CDR3 positions. By default,

546    IMGT aligned CDR1, CDR2, and CDR2.5 amino acids are inferred from TRVB gene names, using the *01

547    allele sequences when allele level information is not available. The CDR3 junction sequences are

548    trimmed 3 amino acids on the N-terminal side and 2 amino acids on the C-terminus, positions that are

549    highly conserved and less crucial for mediation of antigen recognition. For two CDR3s with different

550    lengths, a set of consecutive gaps are inserted at a position in the shorter sequence that minimizes the

551    summed substitution penalties based on a BLOSUM62 substitution matrix. Distances are then the

552    weighted sum of substitution penalties across all CDRs, with the CDR3 penalty weighted three times that

553    of the other CDRs.

554

555    *Optimized TCR-specific radius*

556

557          To find biochemically similar TCRs while maintaining a high level of specificity, we used the

558    packages *tcrdist3* and *tcrsampler* to generate an appropriate set of unenriched antigen-naïve background

559    TCRs. A background repertoire was created for each MIRA set, with each consisting of two parts. First,

560    we combined a set of 100,000 synthetic TCRs generated using the software OLGA (Marcou et al., 2018;

561    Sethna et al., 2019), whose TRBV- and TRBJ-gene frequencies match those in the antigen-enriched

562    repertoire. Second we used 100,000 umbilical cord blood TCRs sampled evenly from 8 subjects

563    (Britanova et al., 2016). This mix balances dense sampling of background sequences near the

564    biochemical neighborhoods of interest with broad sampling of common TCR representative of antigen-

565    naive repertoire. We then adjust for the biased sampling by using the TRBV- and TRBJ-gene frequencies

566    observed in the cord-blood data. The adjustment is a weighting based on the inverse of each TCR's

567    sampling probability. Because we oversampled regions of the "TCR space" near the candidate centroids

568    we were able to estimate the density of the meta-clonotype neighborhoods well below 1 in 200,000.  This

569    is important because ideal meta-clonotypes would be highly specific even in repertoires larger than

570    200,000 sequences. With each candidate centroid, a meta-clonotype was engineered by selecting the

571    maximum distance radius that still controlled the number of neighboring TCRs in the weighted unenriched

572    background to 1 in $10^6$. Candidate centroids that used a TRBV gene that was not in the cord-blood

573    repertoires were excluded from further analysis, since an estimate of gene frequency is required to apply

574    the inverse weighting described above.

575

576    *TCR meta-clonotype MOTIF constraint*

577

578          Radius-optimized meta-clonotypes from antigen-enriched TCRs- provided an opportunity to

579    discover key conserved residues most likely mediating antigen specificity. We developed a "motif"

580    constraint as an optional part of each meta-clonotype definition that limited allowable amino-acid

581    substitutions in highly conserved positions of the CDR3 to those observed in the antigen-enriched TCRs.

582    The motif constraint for each radius-defined meta-clonotype was defined by aligning each of the

583 conformant CDR3 amino-acid sequences to the centroid CDR3. Alignment positions with five or fewer

584 distinct amino acids were considered conserved and added to the motif as a set of possible residues.

585 Thus, the motif constraint is permissive of only specific substitutions in select positions relative to the

586 centroid, however these substitutions are still penalized by the radius constraint. The motif constraint was

587 encoded as a regular expression, with the "." character indicating non-conserved positions and bracketed

588 residues indicating a degenerate position with a set of allowable residues (e.g., "SL[RK][ND]YEQ").

589 Position with gaps, where some sequences are missing a residue, are accommodated by making that

590 position optional (e.g., "SL[RK]?[ND]YEQ").  Since the motif constraints form regular expressions, they

591 can be used to rapidly scan large repertoires for conformant CRs and easily be combined with a radius

592 constraint. When applied to bulk repertoires, the motif constraint eliminates CDR3s that did not match key

593 conserved residues.

594

595 *TCR abundance regression modeling*

596

597 Similar to bulk RNA sequencing data, TCR frequencies are count data drawn from samples of

598 heterogeneous size. Thus we initially attempted to fit a negative binomial model to the data (e.g.,

599 DESEQ2 (Love et al., 2013)). We found that the negative binomial model did not adequately fit TCR

600 counts, which – compared to transcriptomic data – were characterized by (i) more technical zeros due to

601 inevitable under sampling and (ii) even greater biological over-dispersion, which could be due to clonal

602 expansions and HLA genotype diversity. Instead we found that the beta-binomial distribution, which was

603 recently used for TCR abundance modeling (Rytlewski et al., 2019), provided the flexibility needed to

604 adequately fit the TCR data. We used an R package, *corncob*, which provides maximum likelihood

605 methods for inference and hypothesis testing with beta-binomial regression models (Martin et al., 2020).

606 Due to the sparsity of some meta-clonotypes, seven percent of coefficient estimates in regression models

607 had p-values larger than 0.99 (i.e., non-significant) and unreliable high magnitude coefficient estimates.

608 These values are not shown in the horizontal range of the volcano plots. From the p-values for each

609 regression coefficient we computed false-discovery rate (FDR) adjusted q-values and accepted q-values

610 < 0.01 (1%) as statistically significant; adjustment was performed across meta-clonotypes within each

611 MIRA set and within each variable class (e.g., HLA, age, sex, or days since diagnosis). The HLA

612 regression coefficients from the beta-binomial models indicate log-fold differences in meta-clonotype

613 abundance between patients with and without the HLA genotype.

614

615 *Comparison with k-mer based CDR3 features*

616

617 *GLIPH2* (Huang et al., 2020) software *irtools.osx* was applied to 16 antigen-enriched sub-

618 repertoire of TCRs with epitopes with strong prior evidence of restriction to an HLA-A or HLA-B allele to

619 demonstrate how a k-mer based tool might also be used to cluster biochemically similar antigen-specific

620 TCRs to discover potential TCR biomarker features. GLIPH2 generates "global" TCR specificity groups of

621 CDR3s of identical length with a single optional non-conserved position based on enrichment frequency

622 of 'local' continuous 2-mer, 3-mers, and 4-mers. We used the GLIPH2-provided 'ref_CD8_v2.0.txt'

623 background file as a background to identify enriched features. Across epitope-specific MIRA sets, we

624 tested HLA-associations of 812 GLIPH2 pattern ranging from 3 to 11 amino acids in length. The

625 MIRA55:ORF1ab set was chosen for detailed analysis because, among the MIRA sets, it is comprised of

626 CD8+ TCR β-chains activated by a peptide with the strongest evidence of HLA-restriction, primarily HLA-
627 A*01. The MIRA55 set of TCRs, GLIPH2 returned 121 testable public clusters (based on 67 local k-mers,
628 54 global k-mers) associated with CDR3 patterns enriched relative the program's default CD8+ TCR
629 background (GLIPH2 default Fisher's exact test, p-value < 0.001). The GLIPH2 patterns and their
630 associated "specifity group" TRBV gene usages and sequence length were then used to search for
631 conforming TCRs in the 694 bulk unenriched COVID-19 repertoires, allowing comparison to exact and
632 meta-clonotype features. GLIPH2 represents degenerate positions using the "%" character, which we
633 represent throughout this study by the "." character.
634

635 *tcrdist3: Software for TCR repertoire analysis*
636

637 *tcrdist3* is an open-source Python3 package for TCR repertoire analysis and visualization. The
638 core of the package is the TCRdist, a distance metric for relating two TCRs, which has been expanded
639 beyond what was previously published (Dash et al., 2017) to include γδ-TCRs. It has also been re-coded
640 to increase CPU efficiency using *numba*, a high-performance just-in-time compiler. A numba-coded
641 edit/Levenshtein distance is also included for comparison, with the flexibility to accommodate novel TCR
642 metrics as they are developed. The package can accommodate data in standardized format including
643 AIRR, vdjdb exports, MIXCR output, 10x Cell Ranger output or Adaptive Biotechnologies immunoSeq
644 output. The package is well documented including examples and tutorials, with source code available on
645 github.com under an MIT license (http://github.com/kmayerbl/tcrdist3). *tcrdist3* imports modules from
646 several other open-source, pip installable packages by the same authors that support the functionality of
647 *tcrdist3*, while also providing more general utility. Briefly, the novel features of these packages and their
648 relevance for TCR repertoire analysis is described here:
649 *pwseqdist* enables fast and flexible computation of pairwise sequence-based distances using
650 either *numba*-enabled tcrdist and edit distances or any user-coded Python3 metric to relate TCRs; it can
651 also accommodate computation of "rectangular" pairwise matrices: distances between a relatively small
652 set of TCRs with all TCRs in a much larger set (e.g., bulk repertoire). On a modern laptop distances can
653 be computed at a rate of ~70M per minute, per CPU.
654 *tcrsampler* is a tool for sub-sampling large bulk datasets to estimate the frequency of TCRs and
655 TCR neighborhoods in non-antigen-enriched background repertoires. The module comes with large, bulk
656 sequenced, default databases for human TCR α, β, γ and δ and mouse TCR β (Britanova et al., 2016;
657 Ravens et al., 2018; Wirasinha et al., 2018). Datasets were selected because they represented the
658 largest pre-antigen exposure TCR repertoires available; users can optionally supply their own background
659 repertoires when applicable. An important feature of *tcrsampler* is the ability to specify sampling strata; for
660 example, sampling is stratified on individual by default so that results are not biased by on individual with
661 deeper sequencing. Sampling can also be stratified on V and/or J-gene usage to over-sample TCRs that
662 are somewhat similar to the TCR neighborhood of interest. This greatly improves sampling efficiency,
663 since comparing a TCR neighborhood to a background set of completely unrelated TCRs is
664 computationally inefficient; however, we note that it is important to adjust for biased sampling approaches
665 via inverse probability weighting to estimate the frequency of oversampled TCRs in a bulk-sequenced
666 repertoire.
667 *palmotif* is a collection of functions for computing symbol heights for sequence logo plots and
668 rendering them as SVG graphics for integration with interactive HTML visualizations or print publication.

669 Much of the computation is based on existing methods that use either KL-divergence/entropy or odds-
670 ratio based approaches to calculate symbol heights. We contribute a novel method for creating a logo
671 from CDR3s with varying lengths. The target sequences are first globally aligned (parasail C++
672 implementation of Needleman-Wunsch) to a pre-selected centroid sequence (Daily, 2016). For logos
673 expressing relative symbol frequency, background sequences are also aligned to the centroid. Logo
674 computation then proceeds as usual, estimating the relative entropy between target and background
675 sequences at each position in the alignment and the contribution of each symbol. Gaps introduced in the
676 centroid sequence are ignored, while gap symbols in the aligned sequences are treated as an additional
677 symbol.
678

679 **SUPPLEMENTAL TABLES**

680 Table S1        Comparison of selected software tools for clustering TCRs
681 Table S2        MIRA enriched repertoires MIRA0 - MIRA252
682 Table S3        HLA class I alleles capable of presenting the SARS-CoV-2 associated peptides in MIRA
683                 screen
684 Table S4        NetMHCpan4.0 peptide MHC class I binding affinity prediction
685 Table S5        Statistical associations between common HLA genotypes of COVID-19 exposed MIRA
686                 participants and SARS-CoV-2 peptide-enriched TCR repertoires
687 Table S6        SARS-CoV-2 CD8+ meta clonotypes summarized by MIRA enriched repertoire
688 Table S7        SARS-CoV-2 CD8+ meta clonotypes with strong evidence of HLA restriction (n = 1831)
689 Table S8        SARS-CoV-2 CD8+ meta clonotypes with less evidence of HLA restriction (n = 2717)
690 Table S9        HLA associations of GLIPH2 k-mers and tcrdist3 meta-clonotypes
691

692 **SUPPLEMENTAL FIGURES**
693

694 Figure S1       Publicity analysis in MIRA participants of CD8+ TCR β-chain features activated by SARS-
695                 CoV-2 peptide ORF1ab (MIRA55) predicted to bind HLA-A*01.
696 Figure S2       Publicity and breadth analysis of CD8+ TCR β-chain features activated by
697                 SARS-CoV-2 peptide ORF1ab (MIRA55) using tcrdist3 and GLIPH2.
698 Figure S3       Detectable HLA-association and CDR3 probability of generation.


699 **DATA AVAILABILITY**

700 ImmuneRACE data is publicly available: https://immunerace.adaptivebiotech.com/data/. All other TCR
701 data is publicly available from VDJdb (https://vdjdb.cdr3.net/) or the cited research.


702 **SOFTWARE AVAILABILITY**

703 The *tcrdist3* code base used in this analysis is freely available at https://github.com/kmayerb/tcrdist3/ with
704 documented examples at http://tcrdist3.readthedocs.io. *tcrdist3* relies on the Python package *pwseqdist* -
705 freely available at https://github.com/agartland/pwseqdist - for numba-optimized just-in-time compiled
706 versions of the TCRdist measure.

707

## CONTRIBUTIONS

Conceptualization: KM, SS, LC, JCC, AS, JG, TH, PT, PB, AF; Methodology; Software: KM, AF; Validation; Formal analysis; Investigation: KM, AF; Data Curation; Writing – original draft preparation: KM, AF; Writing – review & editing: KM, SS, LC, JCC, AS, JG, TH, PT, PB, AF; Supervision: TH, PT, PB, AF; Funding acquisition: TH, PT, PB, AF, JCC

## ACKNOWLEDGEMENTS

## REFERENCES

Ahmadzadeh M, Pasetto A, Jia L, Deniger DC, Stevanović S, Robbins PF, Rosenberg SA. 2019. Tumor-infiltrating human CD4+ regulatory T cells display a distinct TCR repertoire and exhibit tumor and neoantigen reactivity. *Sci Immunol* **4**. doi:10.1126/sciimmunol.aao4310

Britanova OV, Shugay M, Merzlyak EM, Staroverov DB, Putintseva EV, Turchaninova MA, Mamedov IZ, Pogorelyy MV, Bolotin DA, Izraelson M, Davydov AN, Egorov ES, Kasatskaya SA, Rebrikov DV, Lukyanov S, Chudakov DM. 2016. Dynamics of individual T Cell repertoires: from cord blood to centenarians. *The Journal of Immunology* **196**:5005–5013.

Cao K, Wu J, Li Xuemei, Xie H, Tang C, Zhao X, Wang S, Chen L, Zhang W, An Y, Li Xin, Lin L, Chai R, Fang M, Yue Y, Wang X, Ding Y, Zhou L, Zhao Q, Yang H, Wang J, He S, Liu X. 2020. T-cell receptor repertoire data provides new evidence for hygiene hypothesis of allergic diseases. *Allergy*. doi:10.1111/all.14014

Chiou S-H, Tseng D, Reuben A, Mallajosyula V, Molina IS, Conley S, Wilhelmy J, McSween AM, Yang X, Nishimiya D, Sinha R, Nabet BY, Wang C, Shrager JB, Berry MF, Backhus L, Lui NS, Wakelee HA, Neal JW, Padda SK, Berry GJ, Delaidelli A, Sorensen PH, Sotillo E, Tran P, Benson JA, Richards R, Labanieh L, Klysz DD, Louis DM, Feldman SA, Diehn M, Weissman IL, Zhang J, Wistuba II, Futreal PA, Heymach JV, Garcia KC, Mackall CL, Davis MM. 2021. Global analysis of shared T cell specificities in human non-small cell lung cancer enables HLA inference and antigen discovery. *Immunity* **54**:586-602.e8.

Coles CH, Mulvaney RM, Malla S, Walker A, Smith KJ, Lloyd A, Lowe KL, McCully ML, Martinez Hague R, Aleksic M, Harper J, Paston SJ, Donnellan Z, Chester F, Wiederhold K, Robinson RA, Knox A, Stacey AR, Dukes J, Baston E, Griffin S, Jakobsen BK, Vuidepot A, Harper S. 2020. TCRs with distinct specificity profiles use different binding modes to engage an identical peptide-HLA complex. *J Immunol* **204**:1943–1953.

Daily J. 2016. Parasail: SIMD C library for global, semi-global, and local pairwise sequence alignments. *BMC Bioinformatics* **17**:81.

743  Dash P, Fiore-Gartland AJ, Hertz T, Wang GC, Sharma S, Souquette A, Crawford JC, Clemens EB,
744      Nguyen THO, Kedzierska K, La Gruta NL, Bradley P, Thomas PG. 2017. Quantifiable predictive
745      features define epitope-specific T cell receptor repertoires. *Nature* **547**:89–93.

746  DeWitt WS 3rd, Smith A, Schoch G, Hansen JA, Matsen FA 4th, Bradley P. 2018. Human T cell receptor
747      occurrence patterns encode immune history, genetic background, and receptor specificity. *Elife* **7**.
748      doi:10.7554/eLife.38358

749  Elhanati Y, Sethna Z, Callan CG Jr, Mora T, Walczak AM. 2018. Predicting the spectrum of TCR
750      repertoire sharing with a data-driven model of recombination. *Immunol Rev* **284**:167–179.

751  Emerson RO, DeWitt WS, Vignali M, Gravley J, Hu JK, Osborne EJ, Desmarais C, Klinger M, Carlson
752      CS, Hansen JA, Rieder M, Robins HS. 2017. Immunosequencing identifies signatures of
753      cytomegalovirus exposure history and HLA-mediated effects on the T cell repertoire. *Nat Genet*
754      **49**:659–665.

755  Espejo AP, Akgun Y, Al Mana AF, Tjendra Y, Millan NC, Gomez-Fernandez C, Cray C. 2020. Review of
756      current advances in serologic testing for COVID-19. *Am J Clin Pathol*.

757  Glanville J, Huang H, Nau A, Hatton O, Wagar LE, Rubelt F, Ji X, Han A, Krams SM, Pettus C, Haas N,
758      Arlehamn CSL, Sette A, Boyd SD, Scriba TJ, Martinez OM, Davis MM. 2017. Identifying
759      specificity groups in the T cell receptor repertoire. *Nature* **547**:94–98.

760  Grifoni A, Weiskopf D, Ramirez SI, Mateus J, Dan JM, Moderbacher CR, Rawlings SA, Sutherland A,
761      Premkumar L, Jadi RS, Marrama D, de Silva AM, Frazier A, Carlin AF, Greenbaum JA, Peters B,
762      Krammer F, Smith DM, Crotty S, Sette A. 2020. Targets of T Cell Responses to SARS-CoV-2
763      Coronavirus in Humans with COVID-19 Disease and Unexposed Individuals. *Cell* **181**:1489-
764      1501.e15.

765  Huang H, Wang C, Rubelt F, Scriba TJ, Davis MM. 2020. Analyzing the Mycobacterium tuberculosis
766      immune response by T-cell receptor clustering with GLIPH2 and genome-wide antigen screening.
767      *Nat Biotechnol*. doi:10.1038/s41587-020-0505-4

768  Jurtz V, Paul S, Andreatta M, Marcatili P, Peters B, Nielsen M. 2017. NetMHCpan-4.0: Improved peptide–
769      MHC Class I interaction predictions integrating eluted ligand and peptide binding affinity data. *The
770      Journal of Immunology* **199**:3360–3368.

771  Kato T, Matsuda T, Ikeda Y, Park J-H, Leisegang M, Yoshimura S, Hikichi T, Harada M, Zewde M, Sato
772      S, Hasegawa K, Kiyotani K, Nakamura Y. 2018. Effective screening of T cells recognizing
773      neoantigens and construction of T-cell receptor-engineered T cells. *Oncotarget* **9**:11009–11019.

774  Klinger M, Pepin F, Wilkins J, Asbury T, Wittkop T, Zheng J, Moorhead M, Faham M. 2015. Multiplex
775      identification of antigen-specific t cell receptors using a combination of immune assays and
776      immune receptor sequencing. *PLoS One* **10**:e0141561.

777  Le Bert N, Tan AT, Kunasegaran K, Tham CYL, Hafezi M, Chia A, Chng MHY, Lin M, Tan N, Linster M,
778      Chia WN, Chen MI-C, Wang L-F, Ooi EE, Kalimuddin S, Tambyah PA, Low JG-H, Tan Y-J,
779      Bertoletti A. 2020. SARS-CoV-2-specific T cell immunity in cases of COVID-19 and SARS, and
780      uninfected controls. *Nature* **584**:457–462.

781  Love M, Anders S, Huber W. 2013. Differential analysis of RNA-Seq data at the gene level using the
782      DESeq2 package. *Heidelberg: European Molecular Biology Laboratory (EMBL)*.

783  Lythe G, Callard RE, Hoare RL, Molina-París C. 2016. How many TCR clonotypes does a body maintain?
784      *J Theor Biol* **389**:214–224.

785  Marcou Q, Mora T, Walczak AM. 2018. High-throughput immune repertoire analysis with IGoR. *Nat*
786      *Commun* **9**:561.

787  Martin BD, Witten D, Willis AD. 2020. Modeling microbial abundances and dysbiosis with beta-binomial
788      regression. *Ann Appl Stat* **14**:94–115.

789  McMahan K, Yu J, Mercado NB, Loos C, Tostanoski LH, Chandrashekar A, Liu J, Peter L, Atyeo C, Zhu
790      A, Bondzie EA, Dagotto G, Gebre MS, Jacob-Dolan C, Li Z, Nampanya F, Patel S, Pessaint L,
791      Van Ry A, Blade K, Yalley-Ogunro J, Cabus M, Brown R, Cook A, Teow E, Andersen H, Lewis
792      MG, Lauffenburger DA, Alter G, Barouch DH. 2020. Correlates of protection against SARS-CoV-2
793      in rhesus macaques. *Nature*. doi:10.1038/s41586-020-03041-6

794  Meysman P, De Neuter N, Gielis S, Bui Thi D, Ogunjimi B, Laukens K. 2019. On the viability of
795      unsupervised T-cell receptor sequence clustering for epitope preference. *Bioinformatics* **35**:1461–
796      1468.

797  Murugan A, Mora T, Walczak AM, Callan CG Jr. 2012. Statistical inference of the generation probability of
798      T-cell receptors from sequence repertoires. *Proc Natl Acad Sci U S A* **109**:16161–16166.

799  Nalla AK, Casto AM, Huang M-LW, Perchetti GA, Sampoleo R, Shrestha L, Wei Y, Zhu H, Jerome KR,
800      Greninger AL. 2020. Comparative Performance of SARS-CoV-2 Detection Assays Using Seven
801      Different Primer-Probe Sets and One Assay Kit. *J Clin Microbiol* **58**. doi:10.1128/JCM.00557-20

802  Nolan S, Vignali M, Klinger M, Dines JN, Kaplan IM, Svejnoha E, Craft T, Boland K, Pesesky M,
803      Gittelman RM, Snyder TM, Gooley CJ, Semprini S, Cerchione C, Mazza M, Delmonte OM, Dobbs
804      K, Carreño-Tarragona G, Barrio S, Sambri V, Martinelli G, Goldman JD, Heath JR, Notarangelo
805      LD, Carlson JM, Martinez-Lopez J, Robins HS. 2020. A large-scale database of T-cell receptor
806      beta (TCRβ) sequences and binding associations from natural and synthetic exposure to SARS-
807      CoV-2. *Res Sq*. doi:10.21203/rs.3.rs-51964/v1

808  Pogorelyy MV, Minervina AA, Shugay M, Chudakov DM, Lebedev YB, Mora T, Walczak AM. 2019.
809      Detecting T cell receptors involved in immune responses from single repertoire snapshots. *PLOS*
810      *Biology*. doi:10.1371/journal.pbio.3000314

811  Pogorelyy MV, Shugay M. 2019. A framework for annotation of antigen specificities in high-throughput T-
812      Cell repertoire sequencing studies. *Front Immunol* **10**:2159.

813  Ravens S, Schultze-Florey C, Raha S, Sandrock I, Drenker M, Oberdörfer L, Reinhardt A, Ravens I, Beck
814      M, Geffers R, von Kaisenberg C, Heuser M, Thol F, Ganser A, Förster R, Koenecke C, Prinz I.
815      2018. Publisher Correction: Human γδ T cells are quickly reconstituted after stem-cell
816      transplantation and show adaptive clonal expansion in response to viral infection. *Nature*
817      *Immunology*. doi:10.1038/s41590-018-0054-x

818  Ritvo P-G, Saadawi A, Barennes P, Quiniou V, Chaara W, El Soufi K, Bonnet B, Six A, Shugay M,
819      Mariotti-Ferrandiz E, Klatzmann D. 2018. High-resolution repertoire analysis reveals a major
820      bystander activation of Tfh and Tfr cells. *Proc Natl Acad Sci U S A* **115**:9604–9609.

821  Rytlewski J, Deng S, Xie T, Davis C, Robins H, Yusko E, Bienkowska J. 2019. Model to improve
822      specificity for identification of clinically-relevant expanded T cells in peripheral blood. *PLoS One*
823      **14**:e0213684.

824  Sethna Z, Elhanati Y, Callan CG, Walczak AM, Mora T. 2019. OLGA: fast computation of generation
825      probabilities of B- and T-cell receptor amino acid sequences and motifs. *Bioinformatics* **35**:2974–
826      2981.

827   Sette A, Crotty S. 2020. Pre-existing immunity to SARS-CoV-2: the knowns and unknowns. *Nat Rev*
828        *Immunol* **20**:457–458.

829   Shugay M, Bagaev DV, Turchaninova MA, Bolotin DA, Britanova OV, Putintseva EV, Pogorelyy MV,
830        Nazarov VI, Zvyagin IV, Kirgizova VI, Kirgizov KI, Skorobogatova EV, Chudakov DM. 2015.
831        VDJtools: Unifying Post-analysis of T Cell Receptor Repertoires. *PLoS Comput Biol*
832        **11**:e1004503.

833   Shugay M, Bagaev DV, Zvyagin IV, Vroomans RM, Crawford JC, Dolton G, Komech EA, Sycheva AL,
834        Koneva AE, Egorov ES, Eliseev AV, Van Dyk E, Dash P, Attaf M, Rius C, Ladell K, McLaren JE,
835        Matthews KK, Clemens EB, Douek DC, Luciani F, van Baarle D, Kedzierska K, Kesmir C,
836        Thomas PG, Price DA, Sewell AK, Chudakov DM. 2018. VDJdb: a curated database of T-cell
837        receptor sequences with known antigen specificity. *Nucleic Acids Res* **46**:D419–D427.

838   Snyder TM, Gittelman RM, Klinger M, May DH, Osborne EJ, Taniguchi R, Zahid HJ, Kaplan IM, Dines JN,
839        Noakes MN, Pandya R, Chen X, Elasady S, Svejnoha E, Ebert P, Pesesky MW, De Almeida P,
840        O'Donnell H, DeGottardi Q, Keitany G, Lu J, Vong A, Elyanow R, Fields P, Greissl J, Baldo L,
841        Semprini S, Cerchione C, Mazza M, Delmonte OM, Dobbs K, Carreño-Tarragona G, Barrio S,
842        Imberti L, Sottini A, Quiros-Roldan E, Rossi C, Biondi A, Bettini LR, D'Angio M, Bonfanti P,
843        Tompkins MF, Alba C, Dalgard C, Sambri V, Martinelli G, Goldman JD, Heath JR, Su HC,
844        Notarangelo LD, Martinez-Lopez J, Carlson JM, Robins HS. 2020. Magnitude and dynamics of
845        the T-Cell response to SARS-CoV-2 infection at both individual and population levels. *medRxiv*.
846        doi:10.1101/2020.07.31.20165647

847   Soto C, Bombardi RG, Branchizio A, Kose N, Matta P, Sevy AM, Sinkovits RS, Gilchuk P, Finn JA, Crowe
848        JE Jr. 2019. High frequency of shared clonotypes in human B cell receptor repertoires. *Nature*
849        **566**:398–402.

850   Tan AT, Linster M, Tan CW, Le Bert N, Chia WN, Kunasegaran K, Zhuang Y, Tham CYL, Chia A, Smith
851        GJD, Young B, Kalimuddin S, Low JGH, Lye D, Wang L-F, Bertoletti A. 2021. Early induction of
852        functional SARS-CoV-2-specific T cells associates with rapid viral clearance and mild disease in
853        COVID-19 patients. *Cell Rep* **34**:108728.

854   Thomas PG, Crawford JC. 2019. Selected before selection: A case for inherent antigen bias in the T cell
855        receptor repertoire. *Curr Opin Syst Biol* **18**:36–43.

856   Wang Z, Yang X, Zhou Y, Sun J, Liu X, Zhang J, Mei X, Zhong J, Zhao J, Ran P. 2020. COVID-19
857        severity correlates with weaker T-Cell immunity, hypercytokinemia, and lung epithelium injury. *Am*
858        *J Respir Crit Care Med* **202**:606–610.

859   Weiskopf D, Schmitz KS, Raadsen MP, Grifoni A, Okba NMA, Endeman H, van den Akker JPC,
860        Molenkamp R, Koopmans MPG, van Gorp ECM, Haagmans BL, de Swart RL, Sette A, de Vries
861        RD. 2020. Phenotype and kinetics of SARS-CoV-2-specific T cells in COVID-19 patients with
862        acute respiratory distress syndrome. *Sci Immunol* **5**. doi:10.1126/sciimmunol.abd2071

863   Welsh RM, Selin LK. 2002. No one is naive: the significance of heterologous T-cell immunity. *Nat Rev*
864        *Immunol* **2**:417–426.

865   Wirasinha RC, Singh M, Archer SK, Chan A, Harrison PF, Goodnow CC, Daley SR. 2018. αβ T-cell
866        receptors with a central CDR3 cysteine are enriched in CD8αα intraepithelial lymphocytes and
867        their thymic precursors. *Immunol Cell Biol* **96**:553–561.

868    Wolf K, Hether T, Gilchuk P, Kumar A, Rajeh A, Schiebout C, Maybruck J, Buller RM, Ahn T-H, Joyce S,

869          DiPaolo RJ. 2018. Identifying and tracking low-frequency virus-specific TCR clonotypes using

870          high-throughput sequencing. *Cell Rep* **25**:2369-2378.e4.

871

872

873

874

**FIGURE CAPTIONS**

**Figure 1. TCR meta-clonotype framework and application.** (A) Framework: antigen-enriched repertoires were used together with antigen-unenriched background repertoires to engineer TCR meta-clonotypes that define biochemically similar TCRs based on a centroid TCR and a TCRdist radius. Antigen-enriched TCRs came from CD8+ T cells activated by SARS-CoV-2 peptides that were previously discovered (Nolan et al., 2020) in 62 individuals diagnosed with COVID-19 using MIRA (Multiplex Identification of Antigen-Specific T Cell Receptors Assay, Klinger et al., 2015). With each clonotype from the antigen-enriched TCRs, we used *tcrdist3* to evaluate the repertoire fraction spanned at different TCRdist radii within (i) its antigen-enriched repertoire (black) and (ii) a control V- and J-gene matched, inverse probability weighted background repertoire (purple). The set of antigen-enriched TCRs spanned by the optimal radius were then used to develop an additional meta-clonotype motif constraint based on conserved residues in the CDR3 (see Methods for details). An example logo plots shows the CDR3 β-chain motif formed from TCRs – activated by a SARS-CoV-2 peptide (MIRA55 ORF1ab amino acids 1316:1330, ALRKVPTDNYITTY) – within a TCRdist radius 16 of this meta-clonotype's centroid. (B) Application: TCR meta-clonotypes were used to quantify the frequency of putative SARS-CoV-2 antigen-specific TCRs in a large diverse cohort, from whom bulk TCR repertoires were collected 0-30 days after COVID-19 diagnosis (n=694). Meta-clonotypes were evaluated based on their association with a restricting HLA allele. In most cases, evidence of HLA-restriction was stronger for meta-clonotypes (RADIUS or RADIUS+MOTIF) compared to using exact matches to the centroid TCR (EXACT), demonstrated by lower false-discovery rate (FDR) adjusted q-values and larger HLA regression coefficients in beta-binomial count regression models that account for sequencing depth and control for patient age, sex, and days from diagnosis.

**Figure 2. Experimental enrichment of antigen-specific TCRs.** (A) TCR repertoire subsets obtained by single-cell sorting with peptide-MHC tetramers (data from Dash et al. and Sewell et al. via VDJdb; greens), MIRA peptide stimulation enrichment (MIRA55, MIRA48; purples), or random sub-sampling of umbilical cord blood (1,000 or 10,000 TCRs; blues). Biochemical distances were computed among all pairs of TCRs in each subset using the TCRdist metric. Neighborhoods were formed around each TCR using a variable radius (x-axis) and the percent of TCRs in the set with at least one other TCR within its neighborhood was computed. A radius of zero indicates the proportion of TCRs that have at least one TCR with an identical amino acid sequence (solid square). (B) Analysis of MIRA-enriched repertoires for which the participants contributing the TCRs were significantly enriched with a specific class I HLA allele (Table S5).

911 **Figure 3. Heterogeneous TCR neighborhoods within experimentally antigen-enriched and**
912 **unenriched repertoire subsets.** TCR β-chains from (A) a peptide-MHC tetramer-enriched sub-
913 repertoire, (B) a MIRA peptide stimulation-enriched sub-repertoire, or (C) an umbilical cord blood
914 unenriched repertoire. Within each sub-repertoire, an empirical cumulative distribution function (ECDF)
915 was estimated for each TCR (one line) acting as the centroid of a neighborhood over a range of distance
916 radii (x-axis). Each ECDF shows the proportion of TCRs within the MIRA set with a distance to the
917 centroid less than the indicated radius. ECDF color corresponds to the length of the CDR3-β loop. ECDF
918 curves were randomly shifted by <1 unit along the x-axis to reduce overplotting. Vertical ECDF lines
919 starting at $10^{-4}$ indicate no similar TCRs at or below that radius. Percentage of TCRs with an ECDF
920 proportion < $10^{-3}$ (bottom panels), indicates the percentage of TCRs without, or with very few
921 biochemically similar neighbors at the given radius.

922

923 **Figure 4. Radius-defined neighborhood densities within an antigen-enriched and a synthetic**
924 **background repertoire. (**A) Each TCR in the MIRA55 antigen-enriched sub-repertoire (one line) acts as
925 the centroid of a neighborhood and an empirical cumulative distribution function (ECDF) is estimated over
926 a range of distance radii (x-axis). Each ECDF shows the proportion of TCRs within the MIRA set having a
927 distance to the centroid less than the indicated radius. The ECDF line color corresponds to the TCR
928 generation probability ($P_{gen}$) estimated using OLGA (Sethna et al., 2019). The ECDF curves are randomly
929 shifted by <1 unit along the x-axis to reduce overplotting. The bottom panel shows the percentage of
930 TCRs with an ECDF proportion < $10^{-3}$. (B) Estimated ECDF for each MIRA55 TCR based on the
931 proportion of TCRs in a synthetic background repertoire that are within the indicated radius (x-axis). The
932 synthetic background was generated using 100,000 OLGA-generated TCRs and 100,000 TCRs sub-
933 sampled from umbilical cord blood; sampling was matched to the VJ-gene frequency in the MIRA55 sub-
934 repertoire, with inverse probability weighting to account for the sampling bias (see Methods for details).
935 (C) Antigen-enriched ECDF (y-axis) of one example TCR's neighborhood (red line) plotted against ECDF
936 within the synthetic background (x-axis). Example TCR neighborhood is the same indicated by the red
937 line in (A) and (B). The dashed line indicates neighborhoods that are equally dense with TCRs from the
938 antigen-enriched and unenriched background sub-repertoires.

939

940 **Figure 5.  HLA restriction of TCR clonotypes and meta-clonotypes in bulk sequenced TCRβ**
941 **repertoires of COVID-19 patients.** (A) Percentage of TCR features with a statistically significant (FDR <
942 0.01) association with a restricting HLA allele. We tested for associations between patients' inferred
943 genotype and TCR feature abundance using beta-binomial regression controlling for age, sex, and days
944 since COVID-19 diagnosis. (B) For each clonotype/meta-clonotype, the percent of bulk repertoires from
945 COVID-19 patients (n=694) containing TCRs meeting the criteria defined by (1) EXACT (TCRs matching
946 the centroid TRBV gene and amino acid sequence of the CDR3), (2) RADIUS (TCR centroid with
947 inclusion criteria defined by an optimized TCRdist radius), or (3) RADIUS + MOTIF (inclusion criteria
948 defined by TCR centroid, optimized radius, and the CDR3 motif constraint). See Figure 1 and Methods for
949 details.

950

951

952  **Figure 6. Associations of TCR features with participant age, days post diagnosis, HLA-genotype,**
953  **and sex in TCR β-chain repertoires of COVID-19 patients (n=694).** (A) Beta-binomial regression
954  coefficient estimates (x-axis) and negative $\log_{10}$ false discovery rates (y-axis) for features developed from
955  CD8+ TCRs activated by SARS-CoV-2 MIRA55 ORF1ab amino acids 1636:1647, HTTDPSFLGRY. The
956  abundances of TCR meta-clonotypes are more robustly associated with predicted HLA type than exact
957  clonotypes. (B) Signal strength of enrichment by participant HLA-type (2-digit) of TCR β-chain clonotypes
958  (EXACT) and meta-clonotypes (RADIUS or RADIUS+MOTIF) predicted to recognize additional HLA-
959  restricted SARS-CoV-2 peptides: (i) MIRA48 (ii) MIRA51 (iii) MIRA53 (iv) MIRA55 (v) MIRA110, and (vi)
960  MIRA11 (See Table S6). Models were estimated with counts of productive TCRs matching clonotypes
961  (EXACT) or meta-clonotypes (RADIUS or RADIUS+MOTIF) with the following definitions: (1) EXACT
962  (inclusion of TCRs matching the centroid TRBV gene and amino acid sequence of the CDR3), (2)
963  RADIUS (inclusion criteria defined by a TCR centroid and optimized TCRdist radius), (3) RADIUS +
964  MOTIF (inclusion criteria defined by TCR centroid, optimized radius, and CDR3 motif constraint). See
965  Methods for details.

966

967  **Figure 7. Associations between HLA-genotypes in COVID-19 patients and abundance of epitope**
968  **specific CDR3 k-mers or meta-clonotypes.** (A) Beta-binomial regression coefficient estimates (x-axis)
969  for participant genotype matching a hypothesized restricting HLA allele and negative $\log_{10}$ false discovery
970  rates (y-axis) for features developed from CD8+ TCRs activated by one of 16 HLA-restricted SARS-CoV-
971  2 epitopes found in ORF1ab, ORF3a, nucleocapsid (N), and surface glycoprotein (S). Regression models
972  included age, sex, and days post diagnosis as covariates (not shown). Positive HLA coefficient estimates
973  correspond with greater abundance of the TCR feature in those patients expressing the restricting allele.
974  (B) Distribution of false discovery rates by feature identification method (k-mer local, k-mer global, or
975  meta-clonotype). Larger negative log10-tranformed FDR values (y-axis) indicate more statistically
976  significant associations. Local k-mer (e.g., FRTD) and global k-mer (e.g., SFRTD.YE) were identified
977  using GLIPH2 (Huang et al., 2020) and were used to quantify counts of conforming TCRs in each bulk
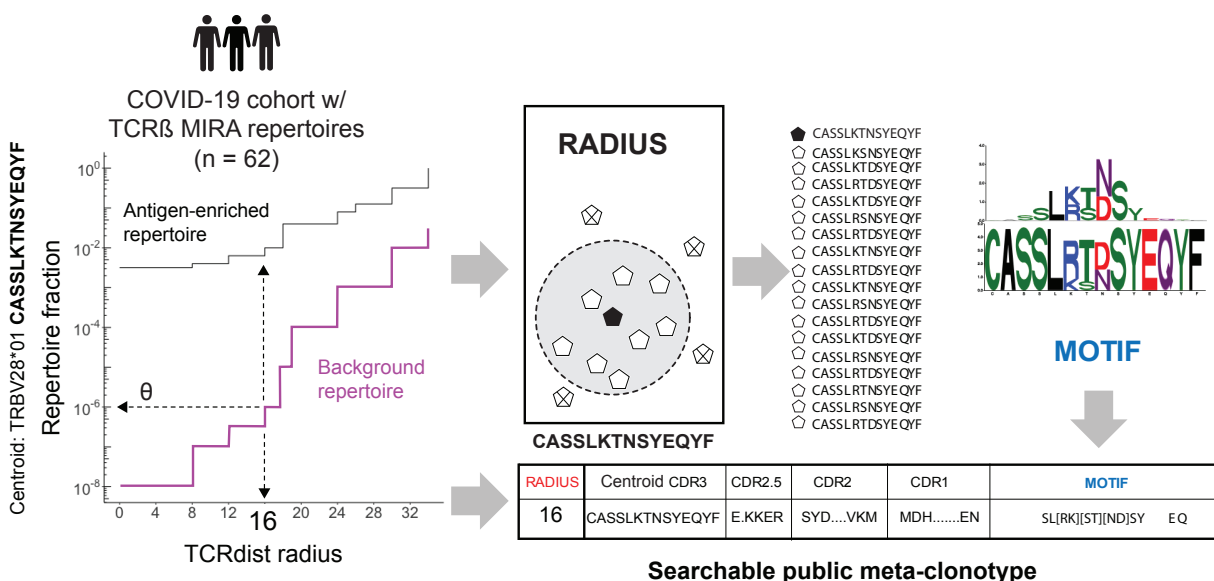978  sequenced COVID-19 repertoire (see Method for details).

979

980  **Figure S1: Publicity analysis in MIRA participants of CD8+ TCR β-chain features activated by**
981  **SARS-CoV-2 peptide ORF1ab (MIRA55) predicted to bind HLA-A*01.** The grid shows all features that
982  were present in 2 or more MIRA participants. TCR feature publicity across individuals was assessed
983  using two methods: (i) tcrdist3 *meta-clonotypes* (rectangles) – inclusion criteria defined by a centroid TCR
984  and all TCRs within an optimized TCRdist radius selected to span $< 10^{-6}$ TCRs in a bulk unenriched
985  background repertoire, and (ii) exact public clonotypes (circles) are defined by matching TRBV gene
986  usage and identical CDR3 amino acid sequence. Per subject, the color-scale shows the meta-clonotype
987  conformant clone with the highest probability of generation ($P_{gen}$). All TCRs captured by a "redundant"
988  meta-clonotypes were completely captured by a higher ranked meta-clonotype. Redundant meta-
989  clonotypes were not subsequently evaluated.

990

991

**Figure S2: Publicity and breadth analysis of CD8+ TCR β-chain features activated by SARS-CoV-2 peptide ORF1ab (MIRA55) using *tcrdist3* and GLIPH2.** TCR feature publicity was determined using two methods for clustering similar TCR sequences: (A) *tcrdist3*-identified meta-clonotypes and (B) GLIPH2 specificity-groups, sets of TCRs with a shared CDR3 k-mer pattern uncommon in the program's default background CD8+ receptor data. Grid fill color shows the breadth – or number of conformant clones – withing each patient's repertoire.

**Figure S3. Detectable HLA-association and CDR3 probability of generation.** We evaluated meta-clonotypes from 17 MIRA sets in a cohort of 694 COVID-19 patients for their association with predicted HLA-restricting alleles. Statistical evidence of the HLA association for each meta-clonotype (RADIUS or RADIUS+MOTIF) and the centroid alone (EXACT) is indicated by the associated false discovery rate (FDR; y-axis) in beta-binomial regressions (see Methods for model details). The probability of generation ($P_{gen}$) of each centroid's CDR3-β was estimated using the software OLGA (x-axis). Using exact matching, only associations with high probability of generation ($P_{gen}$) antigen-specific TCRs are likely to be detected reliably. However, using meta-clonotypes, *tcrdist3* revealed strong evidence of HLA-restriction for TCRs with both high and low probability of generation.
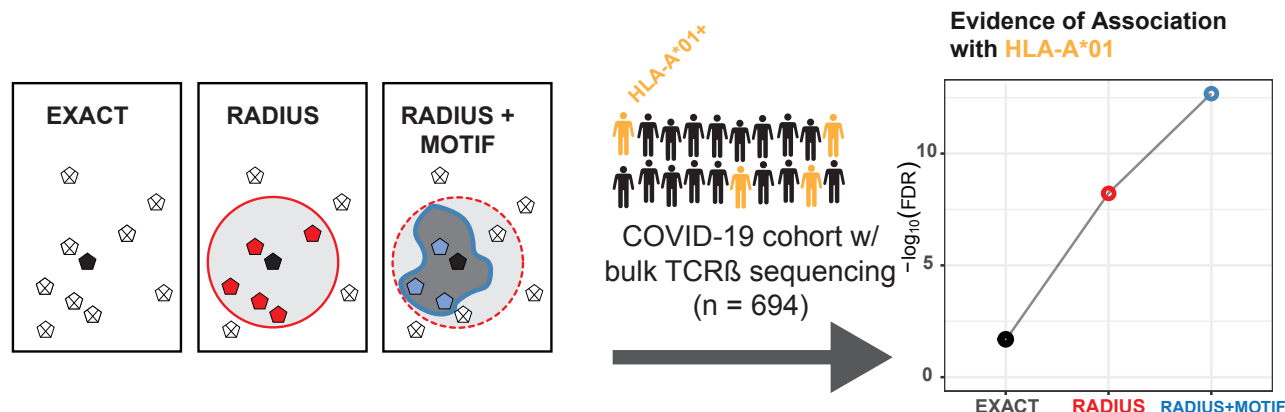
**Figure 1. TCR meta-clonotype framework and application.** (A) Framework: antigen-enriched repertoires were used together with antigen-unenriched background repertoires to engineer TCR meta-clonotypes that define biochemically similar TCRs based on a centroid TCR and a TCRdist radius. Antigen-enriched TCRs came from CD8+ T cells activated by SARS-CoV-2 peptides that were previously discovered (Nolan et al., 2020) in 62 individuals diagnosed with COVID-19 using MIRA (Multiplex Identification of Antigen-Specific T Cell Receptors Assay, Klinger et al., 2015). With each clonotype from the antigen-enriched TCRs, we used *tcrdist3* to evaluate the repertoire fraction spanned at different TCRdist radii within (i) its antigen-enriched repertoire (black) and (ii) a control V- and J-gene matched, inverse probability weighted background repertoire (purple). The set of antigen-enriched TCRs spanned by the optimal radius were then used to develop an additional meta-clonotype motif constraint based on conserved residues in the CDR3 (see Methods for details). An example logo plots shows the CDR3 β-chain motif formed from TCRs – activated by a SARS-CoV-2 peptide (MIRA55 ORF1ab amino acids 1316:1330, ALRKVPTDNYITTY) – within a TCRdist radius 16 of this meta-clonotype's centroid. (B) Application: TCR meta-clonotypes were used to quantify the frequency of putative SARS-CoV-2 antigen-specific TCRs in a large diverse cohort, from whom bulk TCR repertoires were collected 0-30 days after COVID-19 diagnosis (n=694). Meta-clonotypes were evaluated based on their association with a restricting HLA allele. In most cases, evidence of HLA-restriction was stronger for meta-clonotypes (RADIUS or RADIUS+MOTIF) compared to using exact matches to the centroid TCR (EXACT), demonstrated by lower false-discovery rate (FDR) adjusted q-values and larger HLA regression coefficients in beta-binomial count regression models that account for sequencing depth and control for patient age, sex, and days from diagnosis.
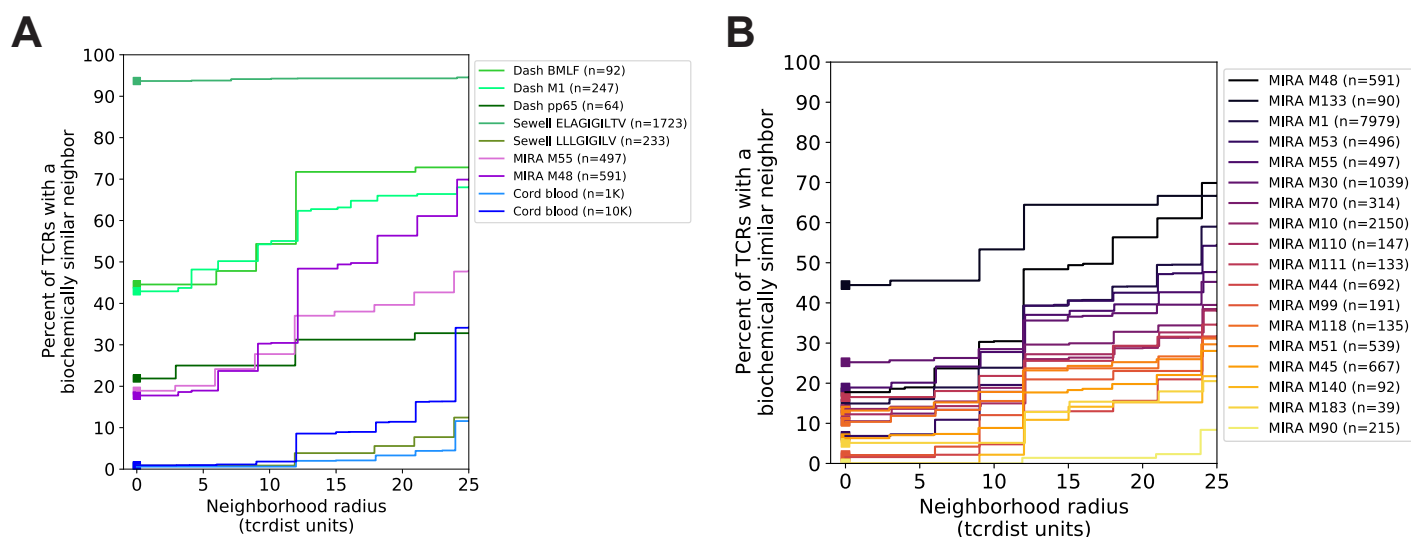
**Figure 2. Experimental enrichment of antigen-specific TCRs.** (A) TCR repertoire subsets obtained by single-cell sorting with peptide-MHC tetramers (data from Dash et al. and Sewell et al. via VDJdb; greens), MIRA peptide stimulation enrichment (MIRA55, MIRA48; purples), or random sub-sampling of umbilical cord blood (1,000 or 10,000 TCRs; blues). Biochemical distances were computed among all pairs of TCRs in each subset using the TCRdist metric. Neighborhoods were formed around each TCR using a variable radius (x-axis) and the percent of TCRs in the set with at least one other TCR within its neighborhood was computed. A radius of zero indicates the proportion of TCRs that have at least one TCR with an identical amino acid sequence (solid square). (B) Analysis of MIRA-enriched repertoires for which the participants contributing the TCRs were significantly enriched with a specific class I HLA allele (Table S5).
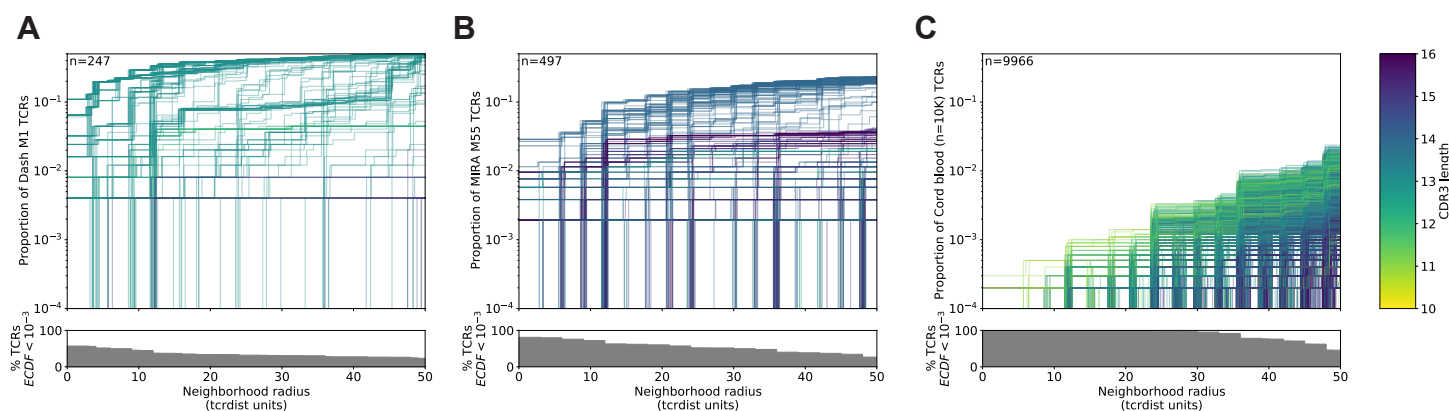


**Figure 3. Heterogeneous TCR neighborhoods within experimentally antigen-enriched and unenriched repertoire subsets.** TCR β-chains from (A) a peptide-MHC tetramer-enriched sub-repertoire, (B) a MIRA peptide stimulation-enriched sub-repertoire, or (C) an umbilical cord blood unenriched repertoire. Within each sub-repertoire, an empirical cumulative distribution function (ECDF) was estimated for each TCR (one line) acting as the centroid of a neighborhood over a range of distance radii (x-axis). Each ECDF shows the proportion of TCRs within the MIRA set with a distance to the centroid less than the indicated radius. ECDF color corresponds to the length of the CDR3-β loop. ECDF curves were randomly shifted by <1 unit along the x-axis to reduce overplotting. Vertical ECDF lines starting at $10^{-4}$ indicate no similar TCRs at or below that radius. Percentage of TCRs with an ECDF proportion < $10^{-3}$ (bottom panels), indicates the percentage of TCRs without, or with very few biochemically similar neighbors at the given radius.

**Figure 4. Radius-defined neighborhood densities within an antigen-enriched and a synthetic background repertoire.** (A) Each TCR in the MIRA55 antigen-enriched sub-repertoire (one line) acts as the centroid of a neighborhood and an empirical cumulative distribution function (ECDF) is estimated over a range of distance radii (x-axis). Each ECDF shows the proportion of TCRs within the MIRA set having a distance to the centroid less than the indicated radius. The ECDF line color corresponds to the TCR generation probability ($P_{gen}$) estimated using OLGA (Sethna et al., 2019). The ECDF curves are randomly shifted by <1 unit along the x-axis to reduce overplotting. The bottom panel shows the percentage of TCRs with an ECDF proportion < $10^{-3}$. (B) Estimated ECDF for each MIRA55 TCR based on the proportion of TCRs in a synthetic background repertoire that are within the indicated radius (x-axis). The synthetic background was generated using 100,000 OLGA-generated TCRs and 100,000 TCRs sub-sampled from umbilical cord blood; sampling was matched to the VJ-gene frequency in the MIRA55 sub-repertoire, with inverse probability weighting to account for the sampling bias (see Methods for details). (C) Antigen-enriched ECDF (y-axis) of one example TCR's neighborhood (red line) plotted against ECDF within the synthetic background (x-axis). Example TCR neighborhood is the same indicated by the red line in (A) and (B). The dashed line indicates neighborhoods that are equally dense with TCRs from the antigen-enriched and unenriched background sub-repertoires.
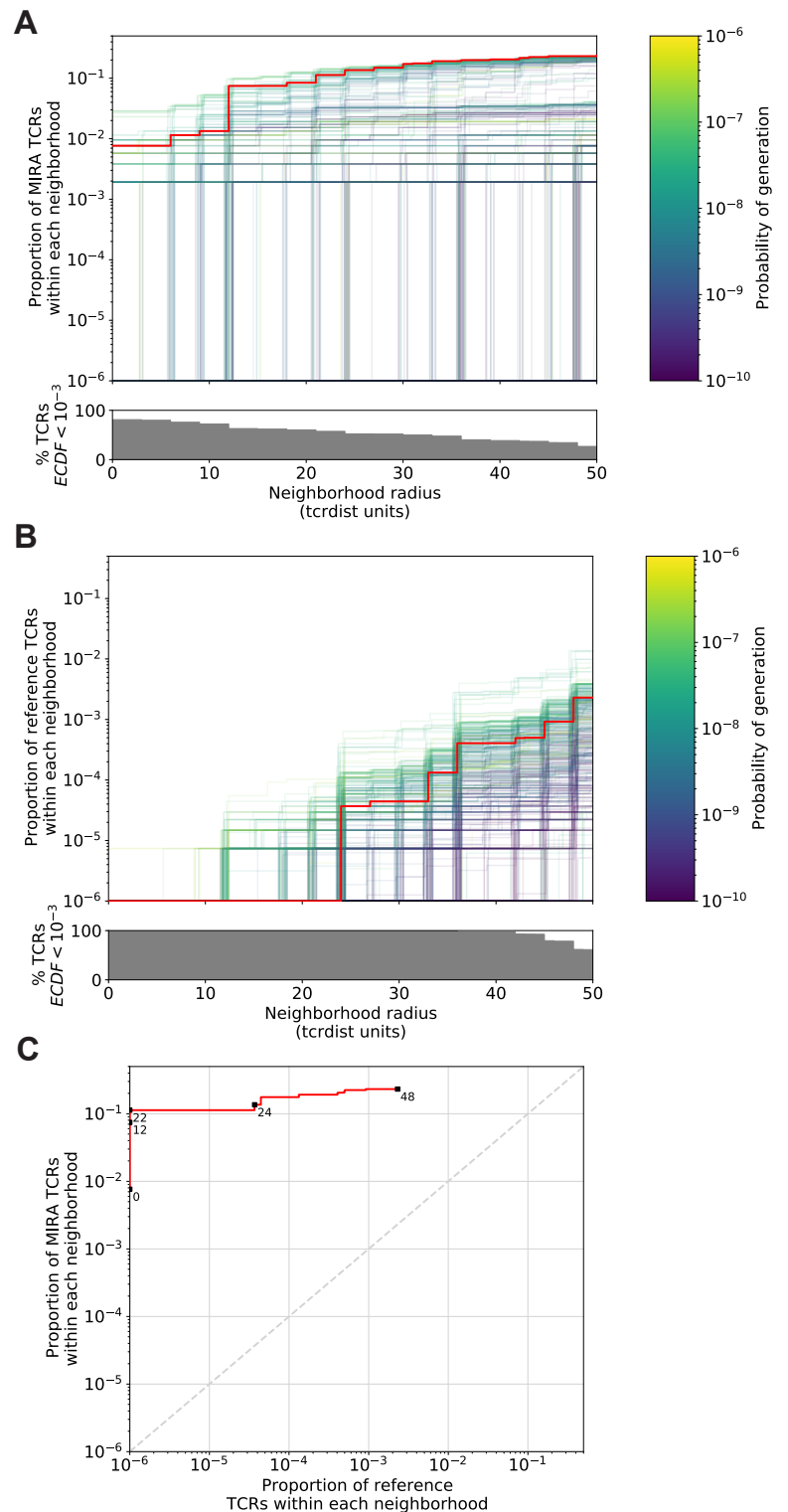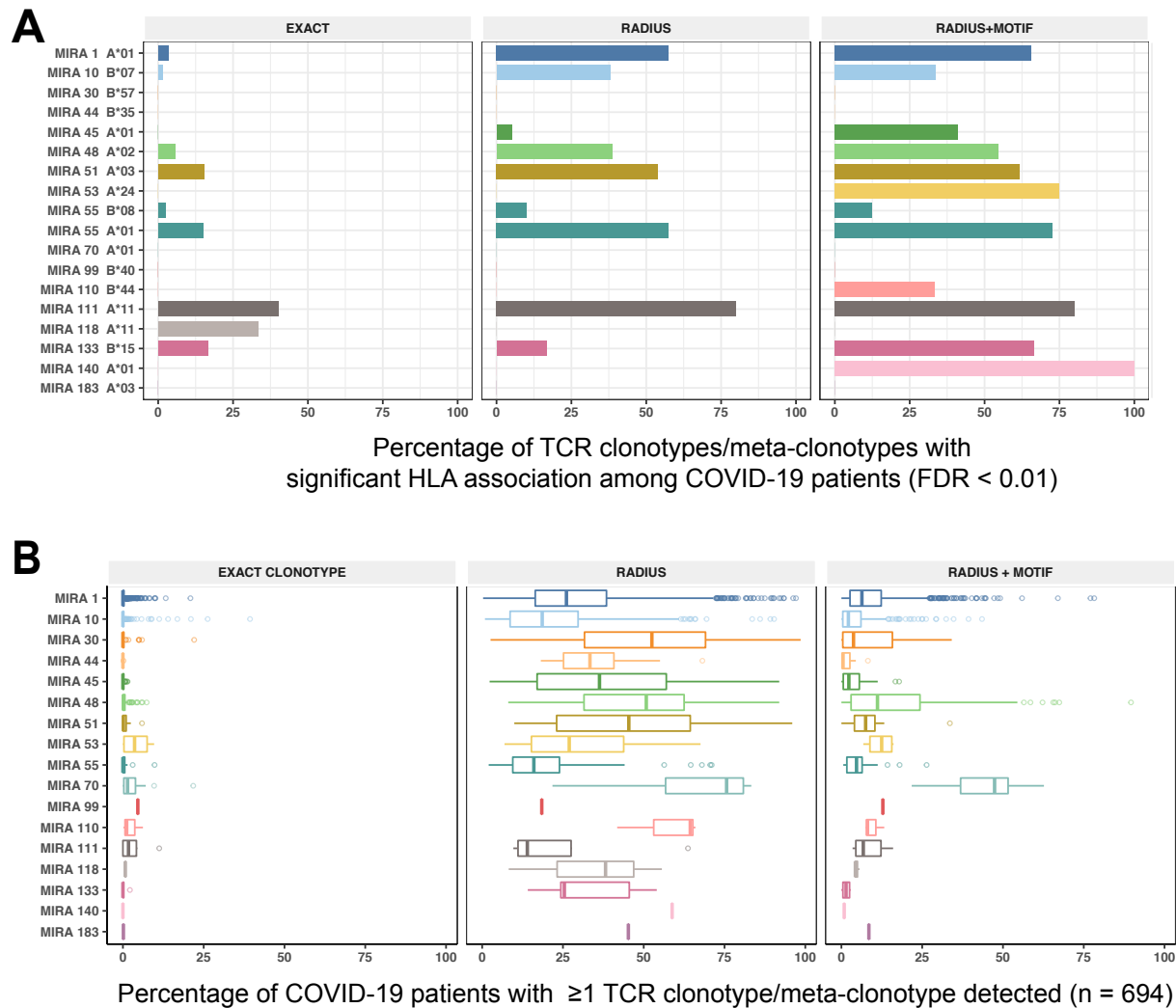
**Figure 5. HLA restriction of TCR clonotypes and meta-clonotypes in bulk sequenced TCRβ repertoires of COVID-19 patients.** (A) Percentage of TCR features with a statistically significant (FDR < 0.01) association with a restricting HLA allele. We tested for associations between patients' inferred genotype and TCR feature abundance using beta-binomial regression controlling for age, sex, and days since COVID-19 diagnosis. (B) For each clonotype/meta-clonotype, the percent of bulk repertoires from COVID-19 patients (n=694) containing TCRs meeting the criteria defined by (1) EXACT (TCRs matching the centroid TRBV gene and amino acid sequence of the CDR3), (2) RADIUS (TCR centroid with inclusion criteria defined by an optimized TCRdist radius), or (3) RADIUS + MOTIF (inclusion criteria defined by TCR centroid, optimized radius, and the CDR3 motif constraint). See Figure 1 and Methods for details.
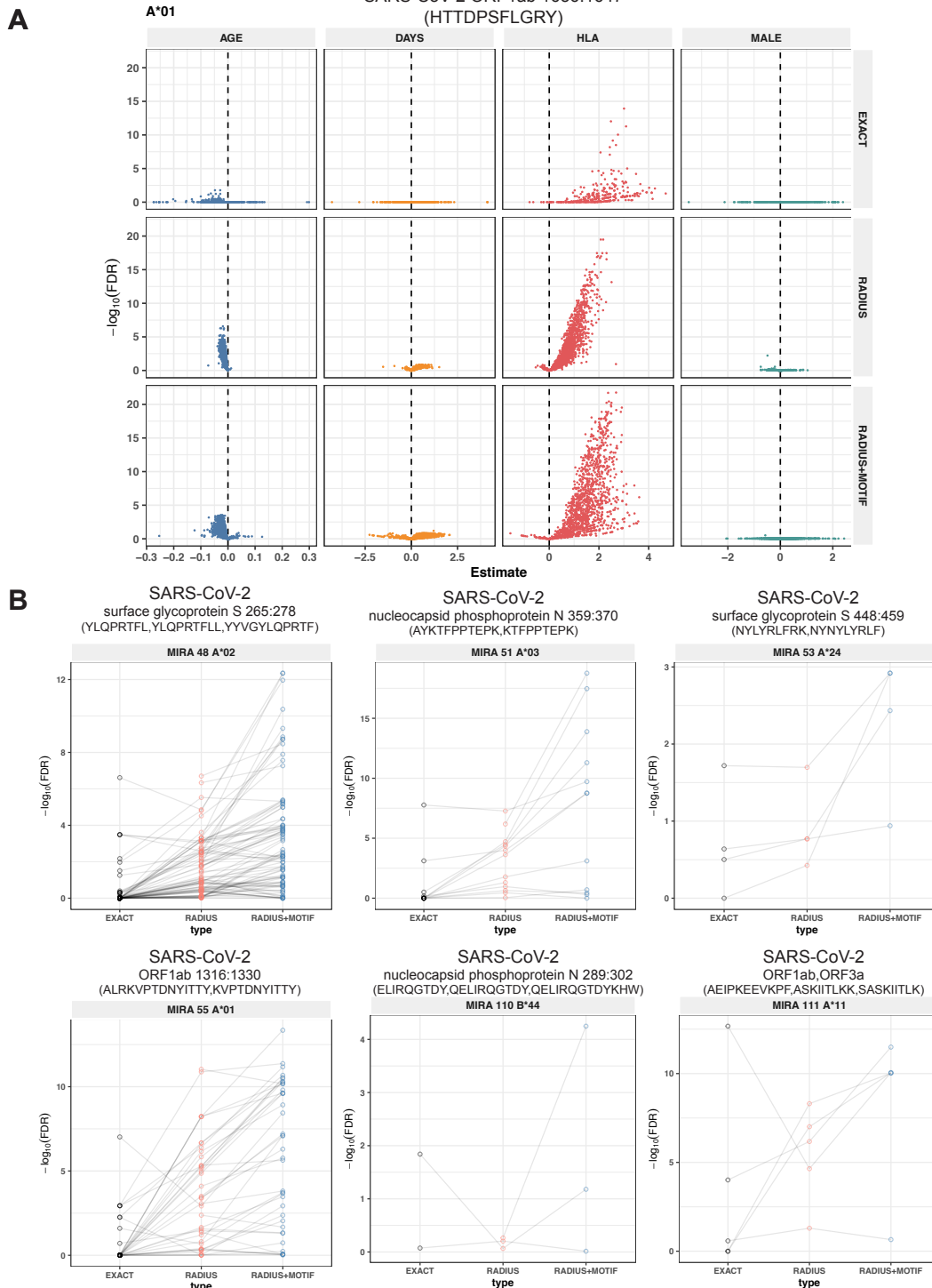
**Figure 6. Associations of TCR features with participant age, days post diagnosis, HLA-genotype, and sex in TCR β-chain repertoires of COVID-19 patients (n=694).** (A) Beta-binomial regression coefficient estimates (x-axis) and negative $\log_{10}$ false discovery rates (y-axis) for features developed from CD8+ TCRs activated by SARS-CoV-2 MIRA55 ORF1ab amino acids 1636:1647, HTTDPSFLGRY. The abundances of TCR meta-clonotypes are more robustly associated with predicted HLA type than exact clonotypes. (B) Signal strength of enrichment by participant HLA-type (2-digit) of TCR β-chain clonotypes (EXACT) and meta-clonotypes (RADIUS or RADIUS+MOTIF) predicted to recognize additional HLA-restricted SARS-CoV-2 peptides: (i) MIRA48 (ii) MIRA51 (iii) MIRA53 (iv) MIRA55 (v) MIRA110, and (vi) MIRA11 (See Table S6). Models were estimated with counts of productive TCRs matching clonotypes (EXACT) or meta-clonotypes (RADIUS or RADIUS+MOTIF) with the following definitions: (1) EXACT (inclusion of TCRs matching the centroid TRBV gene and amino acid sequence of the CDR3), (2) RADIUS (inclusion criteria defined by a TCR centroid and optimized TCRdist radius), (3) RADIUS + MOTIF (inclusion criteria defined by TCR centroid, optimized radius, and CDR3 motif constraint). See Methods for details.
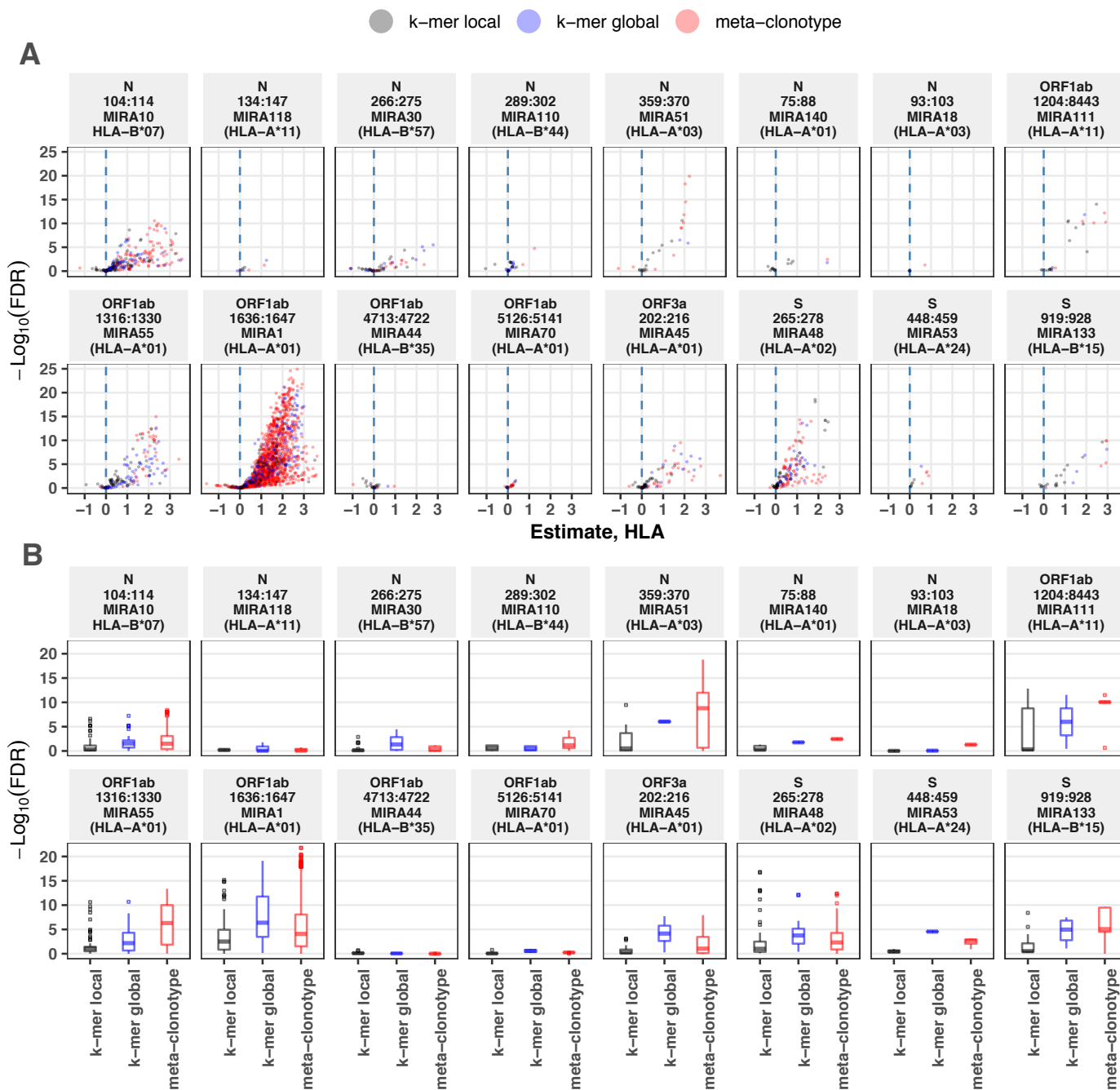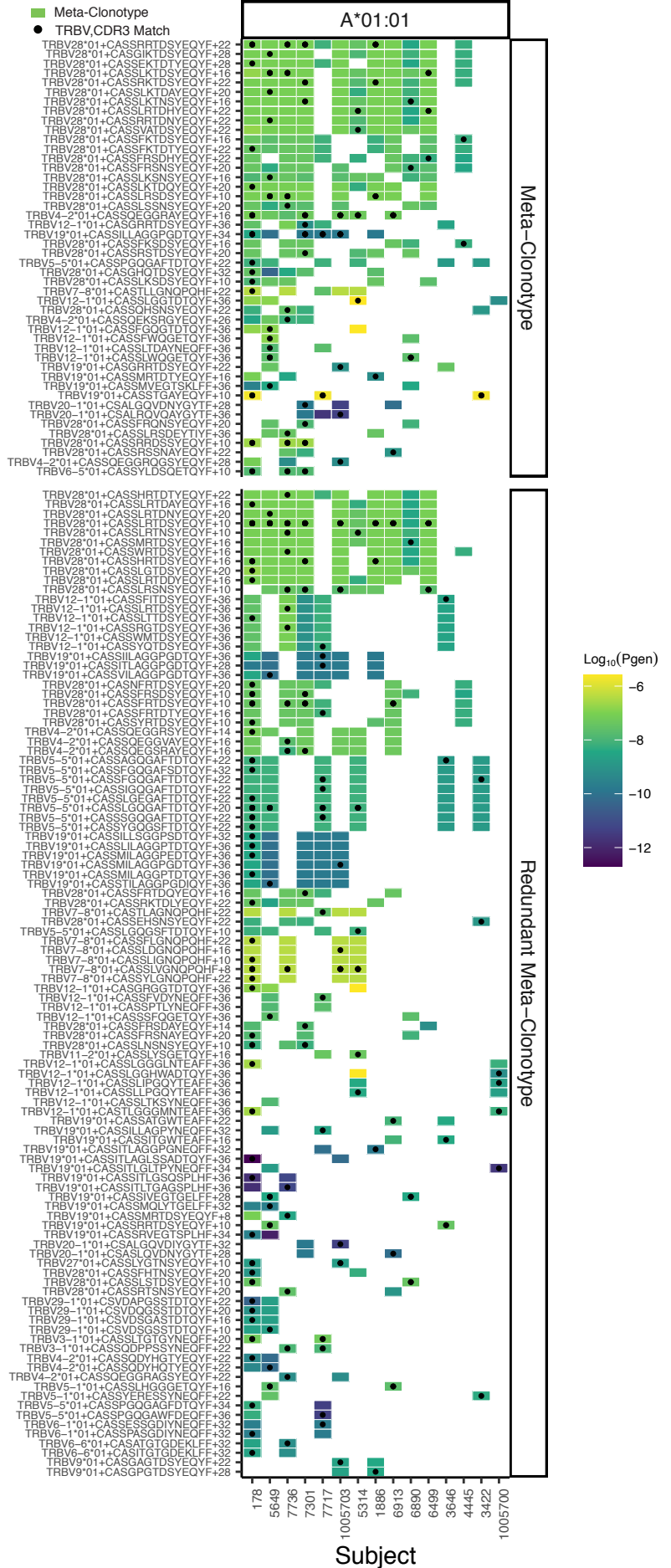
**Figure 7. Associations between HLA-genotypes in COVID-19 patients and abundance of epitope specific CDR3 k-mers or meta-clonotypes.** (A) Beta-binomial regression coefficient estimates (x-axis) for participant genotype matching a hypothesized restricting HLA allele and negative $\log_{10}$ false discovery rates (y-axis) for features developed from CD8+ TCRs activated by one of 16 HLA-restricted SARS-CoV-2 epitopes found in ORF1ab, ORF3a, nucleocapsid (N), and surface glycoprotein (S). Regression models included age, sex, and days post diagnosis as covariates (not shown). Positive HLA coefficient estimates correspond with greater abundance of the TCR feature in those patients expressing the restricting allele. (B) Distribution of false discovery rates by feature identification method (k-mer local, k-mer global, or meta-clonotype (RADIUS+MOTIF)). Larger negative $\log_{10}$-tranformed FDR values (y-axis) indicate more statistically significant associations. Local k-mer (e.g., FRTD) and global k-mer (e.g., SFRTD.YE) were identified using GLIPH2 (Huang et al., 2020) and were used to quantify counts of conforming TCRs in each bulk sequenced COVID-19 reper-toire (see Method for details).

**Figure S1: Publicity analysis in MIRA participants of CD8+ TCR β-chain features activated by SARS-CoV-2 peptide ORF1ab (MIRA55) predicted to bind HLA-A*01.** The grid shows all features that were present in 2 or more MIRA participants. TCR feature publicity across individuals was assessed using two methods: (i) *tcrdist3* meta-clonotypes (rectangles) – inclusion criteria defined by a centroid TCR and all TCRs within an optimized TCRdist radius selected to span < $10^{-6}$ TCRs in a bulk unenriched background repertoire, and (ii) exact public clonotypes (circles) are defined by matching TRBV gene usage and identical CDR3 amino acid sequence. Per subject, the color-scale shows the meta-clonotype conformant clone with the highest probability of generation ($P_{gen}$). All TCRs captured by a "redundant" meta-clonotypes were completely captured by a higher ranked meta-clonotype. Redundant meta-clonotypes were not subsequently evaluated.

**Figure S2: Publicity and breadth analysis of CD8+ TCR β-chain features activated by SARS-CoV-2 peptide ORF1ab (MIRA55) using *tcrdist3* and GLIPH2.** TCR feature publicity was determined using two methods for clustering similar TCR sequences: (A) *tcrdist3*-identified meta-clonotypes and (B) GLIPH2 specificity-groups, sets of TCRs with a shared CDR3 k-mer pattern uncommon in the program's default background CD8+ receptor data. Grid fill color shows the breadth – or number of conformant clones – withing each patient's repertoire.
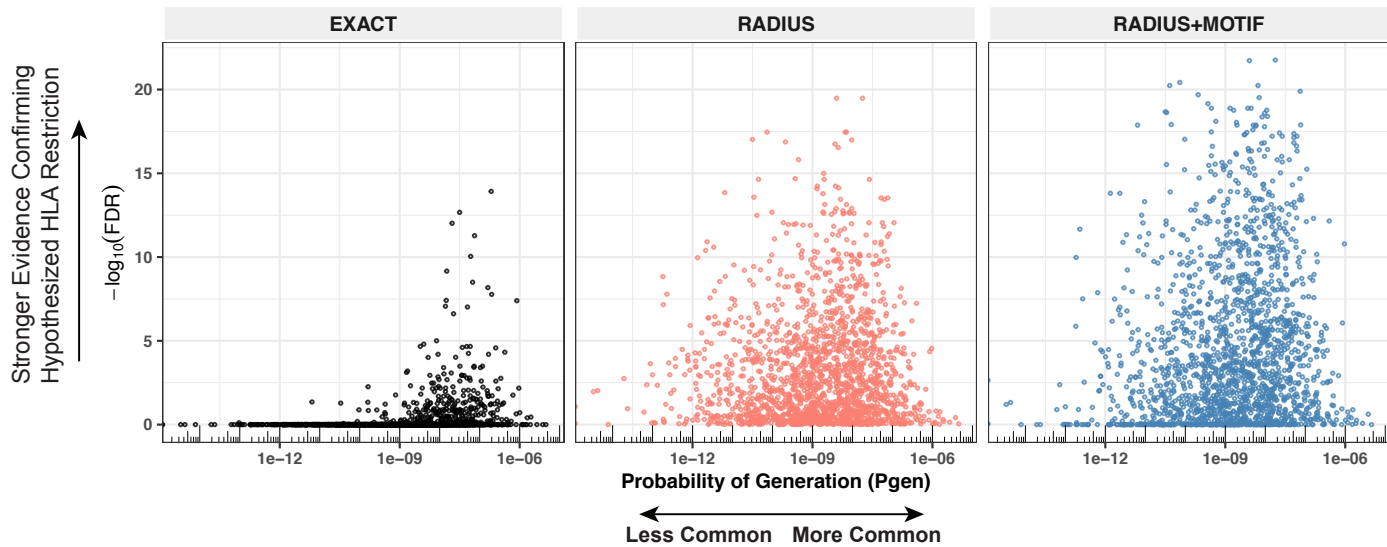
**Figure S3. Detectable HLA-association and CDR3 probability of generation.** We evaluated meta-clonotypes from 17 MIRA sets in a cohort of 694 COVID-19 patients for their association with predicted HLA-restricting alleles. Statistical evidence of the HLA association for each meta-clonotype (RADIUS or RADIUS+MOTIF) and the centroid alone (EXACT) is indicated by the associated false discovery rate (FDR; y-axis) in beta-binomial regressions (see Methods for model details). The probability of generation ($P_{gen}$) of each centroid's CDR3-β was estimated using the software OLGA (x-axis). Using exact matching, only associations with high probability of generation ($P_{gen}$) antigen-specific TCRs are likely to be detected reliably. However, using meta-clonotypes, tcrdist3 revealed strong evidence of HLA-restriction for TCRs with both high and low probability of generation.